Mechanism and Machine Theory 153 (2020) 103985

Contents lists available at ScienceDirect

Mechanism and Machine Theory

journal homepage: www.elsevier.com/locate/mechmachtheory

Nonlinear dynamic modeling of a parallelogram flexure

Majid Baradaran Akbarzadeh[a], Hamid Moeenfard[a,b,*], Shorya Awtar[c]

[a] School of Mechanical Engineering, Ferdowsi University of Mashhad, Mashhad, Khorasan Razavi, Iran
[b] Center of Excellence in Soft Computing and Intelligent Information Processing (SCIIP), Ferdowsi University of Mashhad, Mashhad, Khorasan Razavi, Iran
[c] Department of Mechanical Engineering, University of Michigan, 2350 Hayward Street, Ann Arbor, MI 48109, USA

ARTICLE INFO

Article history:
Received 17 April 2020
Revised 5 June 2020
Accepted 5 June 2020
Available online 6 July 2020

Keywords:
Parallelogram flexure
Dynamic modeling
Eigen value problem
Nonlinear vibration
Analytical solutions

ABSTRACT

The objective of this paper is to propose a novel nonlinear dynamic model for parallelogram flexure mechanisms. First, Hamilton's principle is used to derive the equations of motion of the system and the corresponded boundary conditions. These equations are then employed to find the natural frequencies and mode shapes of the flexure. Afterwards, Lagrange equations are utilized to derive the temporal equations of motion. By eliminating the terms containing time derivatives, the static response of the parallelogram mechanism is studied and the accuracy of the proposed model is verified by comparing load-displacement response of the system with those reported in previous studies. Next, the multiple scales perturbation technique is used to derive analytical expressions for the time response of the flexure. Analytical findings are compared with numerical ones and close agreement is observed. Finally, the response of the system to the harmonic base excitation is analytically studied and frequency responses of the system are obtained in the near resonance case. The presented work can be used as a guideline for vibration analyses of more complex compliant modules.

1. Introduction

Flexure mechanisms provide guided motion via elastic deformation of their elements. These mechanisms have several advantages comparing to their traditional counterparts. For example, flexure mechanisms do not suffer from backlash, wear and friction, don't require any assembly and lubrication, and can provide precise and repeatable motion in specific directions. Due to these specifications, they have been extensively employed in high precision applications such as surgical tools [1,2], micro-grippers [3], micro/nano manipulators [4-6] and energy harvesting devices [7,8].

Beams are the most important components of compliant mechanisms [9-11]. Due to the specific applications such as micro/nano manipulations and energy harvesting systems, the beams in a flexure mechanism undergo relatively large displacements to provide the motion stage with extended travel range. Consequently, geometric nonlinearities are usually activated in them. When these nonlinearities come into play, the analysis of the system becomes more complicated. So far, researchers have employed various methods for analyzing the nonlinear behavior of beams in flexure systems. These methods include the pseudo-rigid body model [12-15], elliptic integral solutions (EIS) [16], beam constraint model (BCM) and the chained BCM (CBCM) [17,18]. The major limitations of the pseudo-rigid body model are its dependence on the loading conditions,

* Corresponding author.
E-mail address: h_moeenfard@um.ac.ir (H. Moeenfard).

https://doi.org/10.1016/j.mechmachtheory.2020.103985
0094-114X/

disability in properly estimating the end slope of the beam, lacking compliance-related characteristics such as elastic and elasto-kinematic effects in the axial direction as well as low accuracy [19]. The EIS on the other hand can be employed for finding the exact solution of the nonlinear form of Euler-Bernoulli beam problem in large deflection ranges (even more than 0.15 of the beam's length) [20]. However, it is very complex and is not a preferred technique for intermediate displacement ranges. The BCM can easily capture load stiffening and elasto-kinematic effects. The results of this method are valid up to deflection ranges of 0.10 to 0.15 of the beam's length [21]. Since the travel range in most flexure mechanisms is less than this amount, the BCM has been widely used in the published literature to obtain the load-displacement relations of compliant units. Awtar and Sen [22] developed a BCM to model the load-displacement behavior of a flexure beam in intermediate displacement range. Their formulation was later used in [23-25] to analyze the static behavior of more complex compliant units. The behavior of the flexure mechanisms can also be studied using CBCM. In this method, the structure is divided into finite elements, whose individual deflection could be considered small [26]. CBCM can properly capture even very large deflections of the compliant units. When using the CBCM, the load-displacement relation of each element has to be stated in terms of the global coordinate system. So, compared with BCM, the major drawback of the CBCM is its tremendous analytical effort required for transforming the load-displacement relations from the element coordinate system to the global one. Moreover, in this technique, the internal loads and displacements has to be eliminated from the element equations, so that the mechanism's behavior can be solely stated in terms of the end loads and stage's displacements which may require much additional analytical attempts.

The performance of the flexure mechanisms usually suffer from the error motions. In an ideal condition, a flexure mechanism shall provide negligible stiffness in the direction of the desired path, while offering infinite stiffness in the directions perpendicular to it. Different strategies can be employed to achieve this ideal condition. For example, a commonly used approach is to stiff an intermediate section in the constitutive beams. It has been shown in different researches [10,20] that an intermediate rigid or even semi-rigid element in the beams of a flexure can improve the planar trajectories of the motion stage. Another technique which can be utilized for improving the motion characteristics of a compliant mechanism is to synthesize the fundamental compliant units either in serial or in parallel. For example, by using two flexure beams in parallel, a P-flexure can be established. Two P-flexures placed in series, form a double parallelogram (DP) flexure, and two parallel DPs creates a paired double parallelogram (DP-DP) flexure. The static behavior of these flexures have been well-studied in the prior arts [10,11,22] and closed-form compact formulations are available for their DoF and DoC stiffnesses as well as their error motions.

As it is observed, most of the analyses carried out in the published literature concern about the static behavior of the flexure mechanisms and their dynamic behavior has not received sufficient attention yet. As these mechanisms are usually designed for large displacement ranges, any investigation of their dynamic behavior should consider geometric nonlinearities, which in turn will severely intricate the analysis. Attempts for studying the dynamic behavior in flexure mechanisms are mostly restricted to the case of simple compliant units such as flexure beams. For example, Moeenfard and Awtar [27] studied the nonlinear vibration of a flexure beam (as a fundamental element in flexure mechanisms) with a tip mass. This work was extended in [28] by considering a variable cross section for the beam and horizontal and axial eccentricity of the tip mass. Silva and Daqaq [29] investigated the nonlinear flexural response of a slender cantilever beam of constant thickness and linearly varying width to a primary resonance excitation. Sayag and Dowell [30] performed a computational and experimental study on a uniform cantilever beam with a tip mass under base excitations. Radgolchin and Moeenfard [31] analytically modeled the nonlinear flexural-extensional vibration of flexure beams with an interconnected compliant element. Dynamic stiffness matrix (DSM) method has also been employed by the researchers to study the vibrational response of different types of flexure beams. Banerjee [32] outlined a general theory for developing the DSM of structural elements. Later, he [33] derived the dynamic stiffness matrix of a uniform rotating thin beam under the presence of an axial force at the outboard end of the beam. Then the application of this method to the free vibration analysis of uniform and non-uniform beams was demonstrated. This work was extended in [34] to include the effect of an arbitrary hub radius. Ling et al. [35] employed the DSM approach to analyze the free vibration of flexure hinges based on non-uniform Timoshenko beam theory.

Except flexure beams, dynamic analyses of more complicated compliant units have also been considered by previous researchers. For example, Zhou et al. [36] addressed the problem of dynamic modeling of a typical flexure stage with application in a micro-machining system. They employed a lumped parameter model for their nonlinear dynamic formulations. Ling [37] presented a two-port dynamic stiffness model to describe the simultaneous kinetostatic and dynamic of some popular bridge-type compliant mechanisms. Pagani et al. [38] presented an exact DSM formulation to study the free vibration characteristics of solid and thin-walled structures using one-dimensional higher-order theories. Tanksale and Gandhi [39] proposed a novel dynamic displacement amplification method using compliant mechanisms. They used a linear lumped parameter model for formulating their dynamic amplifier. Deijl et al. [40] presented theoretical and experimental dynamic of a statically balanced compliant rotational power transmission mechanism, designed based on kinematics of the Oldham coupling. They proposed a fast and flexible generic model based on multi-body dynamics, which facilitated the design and implementation of this compliant transmission couplings in dynamic applications. Their dynamic model was developed using a lumped parameter model and the mass and stiffness distribution were ignored in their research. Zhang et al. [41] presented a novel design on a large range compliant XY nano manipulator with spatial constraints to reduce parasitic motions. Their simulations were based on the transfer function approach which implicitly indicates the linearity assumption in their formulations. Cui et al. [42] presented a linearized lumped parameter dynamic

model for a flexural system with multiple double parallelogram flexure modules. They used their model to provide design recommendations for avoiding complex non-minimum phase zeros in the non-collocated frequency response of the system.

As briefly reviewed, dynamic analyses of basic flexure modules have not been well-investigated in the previous studies. On the other hand, compliant mechanisms are well suited for various applications such as compact and affordable motion stages for semiconductor wafer inspection [43] and micro electro mechanical system scanners for high-speed imaging [44]. In these applications, the flexure system experiences severe dynamic movements and the designer has to simultaneously achieve large range, high precision, and high-speed [42]. So, the prior knowledge of the dynamic model for these systems will help the designer to ensure stability and robustness of the feedback control system with hardware in the loop. Among a few studies about the dynamic modeling of flexure modules, lumped parameter models have been paid more attention. The accuracy of lumped models can be improved by taking the distribution of mass and stiffness into account. So, as a starting point for broader investigations, in this paper, we will propose a novel dynamic model for a P-flexure. The proposed procedure considers the effect of geometric nonlinearities and eccentricity of the stage. The problem is first modeled using the Hamilton's principle. Then, the mode shapes of the system are derived and the effect of different design parameters on the natural frequencies of the system are studied. Moreover, by using a single mode assumption, the nonlinear free and forced vibration of the P-flexure is analytically formulated.

2. Mathematical modeling

A P-flexure with two identical flexure beams and with dimensional specifications shown in Fig. 1 is considered. In this figure, $2\hat{b}$ and L are respectively the thickness and the length of the flexure beams and $2\hat{t}_m$ and $2\hat{d}$ are some geometrical parameters specifying the dimensions of the stage. The system is assumed to be under harmonic base excitation of $\hat{\mathfrak{z}}(\hat{t}) = \hat{\mathbb{Z}}_b \sin\Omega\hat{t}$. In this section, by employing Hamilton's principle, the nonlinear governing partial differential equations of motion of the system will be derived.

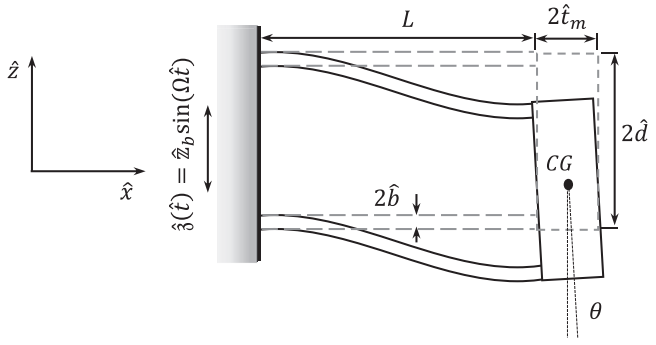

Fig. 1. Schematic view of a P-flexure.

Based on the Hamilton's principle [45]

$$\int_{\hat{t}_1}^{\hat{t}_2} \left(\delta\hat{T} - \delta\hat{\pi} + \delta\hat{W}_{ext}\right) d\hat{t} = 0 \tag{1}$$

where in this equation, δ is the variation operator, $\hat{t}_1$ and $\hat{t}_2$ are two arbitrary times, $\hat{T}$ and $\hat{\pi}$ are the total kinetic and potential energies of the system respectively and $\delta\hat{W}_{ext}$ is the virtual work done by non-conservative loads applied to the system.

Flexure mechanisms can be designed for relatively large range positioning applications. So, their stiffness in the transverse direction (in this case $\hat{z}$) shall be minimum. Consequently, these mechanisms are made up of long slender beams to facilitate movement in the transverse direction. These thin beams can be accurately modeled via Euler-Bernoulli beam theory which have already been extensively employed for simulating static and dynamic behavior of slender flexure beams [28]. Based on this theory, the energy associated with the rotation of the beam's cross sections is negligible compared to the corresponded translational energy.

Large range displacements in flexure mechanisms activate the geometric nonlinearities in the system. The nonlinear von-Karman strain in an infinitesimal element of the Euler-Bernoulli beams in Fig. 1 is as [23,46,47]

$$\varepsilon_{\hat{x}\hat{x},j} = \frac{\partial\hat{u}_j}{\partial\hat{x}} + \frac{1}{2}\left(\frac{\partial\hat{w}_j}{\partial\hat{x}}\right)^2 - \hat{z}\frac{\partial^2\hat{w}_j}{\partial\hat{x}^2}, \qquad j = 1, 2 \tag{2}$$

Please note that hereafter in this paper, the lower beam in Fig. 1 is called the first and the upper one is mentioned as the second beam. Moreover, in Eq. (2), $\hat{u}_j$ and $\hat{w}_j$ are respectively the axial and transversal displacements of an element

placed at a distance $\hat{z}$ from the neutral axis of the j'th beam. If the tip transverse deflection of the beams in the P-flexure is less than 10% to 15% of the beams length, the von-Karman strain can accurately model the geometric nonlinearities in the system.

The total strain energy of the P-flexure shown in Fig. 1 can be obtained by simply adding the strain energies of constitutive beams as

$$\hat{\pi} = \frac{E}{2}\sum_{j=1}^{2}\iiint_{\hat{V}} \hat{\varepsilon}_{\hat{x}\hat{x},j}^{2}\, d\hat{V} \tag{3}$$

In Eq. (3), E and $\hat{V}$ are the Young's modulus of elasticity and the volume of both beams respectively. By performing mathematical simplifications, the above equation can be simplified as [28]

$$\hat{\pi} = \frac{1}{2EA}\sum_{j=1}^{2}\int_0^L \hat{N}_j^2(\hat{x},\hat{t})\, d\hat{x} + \frac{EI}{2}\sum_{j=1}^{2}\int_0^L \left(\frac{\partial^2 \hat{w}_j(\hat{x},\hat{t})}{\partial \hat{x}^2}\right)^2 d\hat{x} \tag{4}$$

in which A and I are respectively the area and the second moment of area around the neutral axis of each beam's cross section. Moreover, $\hat{N}_j(\hat{x},\hat{t})$ is defined as

$$\hat{N}_j(\hat{x},\hat{t}) = EA\left(\frac{\partial \hat{u}_j(\hat{x},\hat{t})}{\partial \hat{x}} + \frac{1}{2}\left(\frac{\partial \hat{w}_j(\hat{x},\hat{t})}{\partial \hat{x}}\right)^2\right), \qquad j = 1,2 \tag{5}$$

It can be shown that if the axial inertia of the beam is negligible compared to the transverse one, then $\hat{N}_j(\hat{x},\hat{t})$ would have no spatial dependence and can be expressed as given in Eq. (6) [27,28]. In derivation of (6), we have implicitly assumed that the area of cross section of beams in Fig. 1 is constant.

$$\hat{N}_j(\hat{x},\hat{t}) = \frac{EA}{L}\left(\hat{u}_j(L,\hat{t}) + \frac{1}{2}\int_0^L \left(\frac{\partial \hat{w}_j(\hat{x},\hat{t})}{\partial \hat{x}}\right)^2 d\hat{x}\right), \qquad j = 1,2 \tag{6}$$

By substituting (6) into (4), the final form of the potential energy of the system is derived as

$$\hat{\pi} = \frac{EA}{2L}\sum_{j=1}^{2}\left(\hat{u}_j(L,\hat{t}) + \frac{1}{2}\int_0^L \left(\frac{\partial \hat{w}_j(\hat{x},\hat{t})}{\partial \hat{x}}\right)^2 d\hat{x}\right)^2 + \frac{EI}{2}\sum_{j=1}^{2}\int_0^L \left(\frac{\partial^2 \hat{w}_j(\hat{x},\hat{t})}{\partial \hat{x}^2}\right)^2 d\hat{x} \tag{7}$$

The kinetic energy of the P-flexure $\hat{T}$, is composed of the kinetic energies of the beams and that of the stage.

$$\hat{T} = \hat{T}_{beams} + \hat{T}_{Mass} \tag{8}$$

Considering the axial and transversal motions of the beams, their kinetic energy can be easily calculated by

$$\hat{T}_{beam} = \frac{\rho A}{2}\sum_{j=1}^{2}\int_0^L \left[\frac{\partial}{\partial \hat{t}}\left(\hat{\delta}(\hat{t}) + \hat{w}_j(\hat{x},\hat{t})\right)\right]^2 d\hat{x} + \frac{\rho A}{2}\sum_{j=1}^{2}\int_0^L \left(\frac{\partial \hat{u}_j(\hat{x},\hat{t})}{\partial \hat{t}}\right)^2 d\hat{x} \tag{9}$$

in which ρ is the volumetric density of the beams. Moreover, assuming the rotation of the stage to be θ and the displacements of its center of gravity along the $\hat{x}$ and $\hat{z}$ axes to be $\hat{u}_{CG}$ and $\hat{w}_{CG}$ respectively, the total kinetic energy of the stage can be expressed as

$$\hat{T}_{Mass} = \frac{1}{2}\hat{M}\left\{\left(\frac{d\hat{u}_{CG}(\hat{t})}{d\hat{t}}\right)^2 + \left(\dot{\hat{\delta}}(\hat{t}) + \frac{d\hat{w}_{CG}(\hat{t})}{d\hat{t}}\right)^2\right\} + \frac{1}{2}\hat{J}_{CG}\dot{\theta}^2(\hat{t}) \tag{10}$$

in which $\hat{M}$ and $\hat{J}_{CG}$ are respectively the mass and the mass moment of inertia of the stage around its center of gravity. Finally, by substituting the kinetic energies of the flexure beams (Eq. (9)) and the stage (Eq. (10)) in (8), the total kinetic energy of the system is derived as

$$\begin{aligned}\hat{T} = {} & \frac{\rho A}{2}\sum_{j=1}^{2}\int_0^L \left[\frac{\partial}{\partial \hat{t}}\left(\hat{\delta}(\hat{t}) + \hat{w}_j(\hat{x},\hat{t})\right)\right]^2 d\hat{x} + \frac{\rho A}{2}\sum_{j=1}^{2}\int_0^L \left(\frac{\partial \hat{u}_j(\hat{x},\hat{t})}{\partial \hat{t}}\right)^2 d\hat{x} \\ & + \frac{1}{2}\hat{M}\left\{\left(\frac{d\hat{u}_{CG}(\hat{t})}{d\hat{t}}\right)^2 + \left(\dot{\hat{\delta}}(\hat{t}) + \frac{d\hat{w}_{CG}(\hat{t})}{d\hat{t}}\right)^2 + \hat{\kappa}^2\dot{\theta}^2(\hat{t})\right\}\end{aligned} \tag{11}$$

in which $\hat{\kappa}$ is the gyration radius of the stage around its center of gravity.

To account for modal damping of the P-flexure, we assume the whole system is vibrating in a viscously damped media with a damping per unit length of $\hat{C}$. So, the virtual work done by non-conservative damping forces can be found as

$$\delta\hat{W}_{ext}^{(\hat{C})} = -\int_0^L \hat{C}\frac{\partial\hat{w}_j(\hat{x},\hat{t})}{\partial\hat{t}}\delta\hat{w}_j(\hat{x},\hat{t})d\hat{x}, \qquad j=1,2 \tag{12}$$

Moreover, the virtual work done by external actuating forces $\hat{F}_{\hat{x}}$ and $\hat{F}_{\hat{z}}$ applied to the stage's center in the $\hat{x}$ and $\hat{z}$ directions are simply as

$$\delta\hat{W}_{ext}^{(\hat{F})} = \hat{F}_{\hat{x}}\delta\hat{u}_{CG} + \hat{F}_{\hat{z}}\delta\hat{w}_{CG} \tag{13}$$

By applying the variation operator on (4) and (11) and substituting the results along with (12) into (1), while employing the fundamental lemma of variational calculus [48], the partial differential equations of motion as well as the natural boundary conditions of the system are obtained. To present these equations more compactly, the following normalized variables are introduced.

$$\begin{aligned} &x = \frac{\hat{x}}{L}, \quad w_j = \frac{\hat{w}_j}{L}, \quad u_j = \frac{\hat{u}_j}{L}, \quad t = \hat{t}\sqrt{\frac{EI}{\rho AL^4}} \\ &t_m = \frac{\hat{t}_m}{L}, \quad d = \frac{\hat{d}}{L}, \quad b = \frac{\hat{b}}{L}, \quad \kappa = \frac{\hat{\kappa}}{L}, \quad \mathfrak{z} = \frac{\hat{\mathfrak{z}}}{L} \\ &C = \frac{\hat{C}L^2}{\sqrt{\rho AEI}}, \quad \mathscr{B} = \frac{AL^2}{I}, \quad M = \frac{\hat{M}}{\rho AL} \end{aligned} \tag{14}$$

Using these dimensionless variables while assuming the flexure beams to have constant and identical physical and geometrical specifications, the governing PDEs of motion become as

$$\begin{aligned} &\frac{\partial^4 w_j(x,t)}{\partial x^4} + C\frac{\partial w_j(x,t)}{\partial t} - \mathscr{B}\frac{\partial}{\partial x}\left(\frac{\partial w_j(x,t)}{\partial x}\left(\frac{\partial u_j(x,t)}{\partial x} + \frac{1}{2}\left(\frac{\partial w_j(x,t)}{\partial x}\right)^2\right)\right) \\ &\qquad + \frac{\partial^2}{\partial t^2}\left(\mathfrak{z}(t) + w_j(x,t)\right) = 0, \qquad j=1,2 \end{aligned} \tag{15}$$

$$\frac{\partial^2 u_j(x,t)}{\partial t^2} - \mathscr{B}\frac{\partial}{\partial x}\left(\frac{\partial u_j(x,t)}{\partial x} + \frac{1}{2}\left(\frac{\partial w_j(x,t)}{\partial x}\right)^2\right) = 0, \qquad j=1,2 \tag{16}$$

Also, the natural boundary conditions of the system are obtained as

$$M\frac{d^2 u_{CG}}{dt^2} + \mathscr{B}\sum_{j=1}^{2}\left(\frac{\partial u_j}{\partial x} + \frac{1}{2}\left(\frac{\partial w_j}{\partial x}\right)^2\right)\Bigg|_{x=1} = 0 \tag{17}$$

$$M\frac{d^2 w_{CG}}{dt^2} + \sum_{j=1}^{2}\left\{\mathscr{B}\frac{\partial w_j}{\partial x}\left(\frac{\partial u_j}{\partial x} + \frac{1}{2}\left(\frac{\partial w_j}{\partial x}\right)^2\right) - \left(\frac{\partial^3 w_j}{\partial x^3}\right)\right\}_{x=1} = -M\frac{d^2\mathfrak{z}(t)}{dt^2} \tag{18}$$

$$\begin{aligned} &M\kappa^2\frac{d^2}{dt^2}\left(\frac{\partial w_1}{\partial x}\Big|_{x=1}\right) + \left\{\sum_{j=1}^{2}\frac{\partial^2 w_j}{\partial x^2} + \mathscr{B}\sum_{j=1}^{2}\left(\frac{\partial u_j}{\partial x} + \frac{1}{2}\left(\frac{\partial w_j}{\partial x}\right)^2\right)\left(t_m\sin\left(\frac{\partial w_j}{\partial x}\right)\right.\right. \\ &\quad \left. + (-1)^{j-1}(d-b)\cos\left(\frac{\partial w_j}{\partial x}\right)\right) + \sum_{j=1}^{2}\left(\mathscr{B}\frac{\partial w_j}{\partial x}\left(\frac{\partial u_j}{\partial x} + \frac{1}{2}\left(\frac{\partial w_j}{\partial x}\right)^2\right) - \frac{\partial^3 w_j}{\partial x^3}\right) \\ &\quad \left.\times\left(-t_m\cos\left(\frac{\partial w_j}{\partial x}\right) + (-1)^{j-1}(d-b)\sin\left(\frac{\partial w_j}{\partial x}\right)\right)\right\}_{x=1} = 0 \end{aligned} \tag{19}$$

Moreover, the kinematic boundary conditions for this system are as

$$u_j(0,t) = w_j(0,t) = \frac{\partial w_j}{\partial x}\Big|_{x=0} = 0, \qquad j=1,2 \tag{20}$$

$$\frac{\partial w_1}{\partial x}\Big|_{x=1} = \frac{\partial w_2}{\partial x}\Big|_{x=1} \tag{21}$$

$$u_1(1,t) = u_2(1,t) + 2(d-b)\sin\left(\left.\frac{\partial w_1}{\partial x}\right|_{x=1}\right) \tag{22}$$

$$w_1(1,t) = w_2(1,t) \tag{23}$$

Eq. (20) is reflecting the clamped boundary conditions of the system. Eq. (21) denotes the fact that the slope of both flexure beams at their connecting point to the stage are the same. Also, Eqs. (22) and (23) can be easily derived from kinematical constraints in Fig. 1.

3. Natural frequencies and mode shapes

The dynamic behavior of linear [45] and nonlinear [47] continuous systems can be approximated by linear combination of their mode-shapes. The mode-shape of a dynamic system is a state of in or out of phase movement of the corresponded linear un-damped homogenous system, in which all elements are vibrating with the same frequency (called the natural frequency), but not necessarily the same amplitude. Assuming the system under study is oscillating in its n'th mode with the corresponded natural frequency of ω_n and denoting the transverse and axial displacements of the j'th beam in this specific mode by $\varphi_j^{(n)}(x)$ and $\psi_j^{(n)}(x)$ respectively, one can say that

$$w_j^{(n)}(x,t) = \varphi_j^{(n)}(x)\exp(I\omega_n t) \tag{24}$$

$$u_j^{(n)}(x,t) = \psi_j^{(n)}(x)\exp(I\omega_n t) \tag{25}$$

where $I = \sqrt{-1}$.

By substituting (24) and (25) into the linearized, un-damped and homogenous form of (15) and (16), we'll get

$$\frac{d^4\varphi_j^{(n)}(x)}{dx^4} - \omega_n^2\varphi_j^{(n)}(x) = 0, \qquad j = 1,2 \tag{26}$$

$$\mathscr{B}\frac{d^2\psi_j^{(n)}(x)}{dx^2} + \omega_n^2\psi_j^{(n)}(x) = 0, \qquad j = 1,2 \tag{27}$$

Moreover, by employing (24) and (25) into the homogeneous linearized natural and kinematic boundary conditions (17)-(23), the following equations are derived.

Natural boundary conditions

$$\mathscr{B}\sum_{j=1}^{2}\left.\frac{d\psi_j^{(n)}}{dx}\right|_{x=1} + M\omega_n^2\left((d-b)\left.\frac{d\varphi_1^{(n)}}{dx}\right|_{x=1} - \psi_1^{(n)}(1)\right) = 0, \quad j = 1,2 \tag{28}$$

$$\sum_{j=1}^{2}\left.\frac{d^3\varphi_j^{(n)}}{dx^3}\right|_{x=1} + M\omega_n^2\left(t_m\left.\frac{d^3\varphi_1^{(n)}}{dx^3}\right|_{x=1} + \varphi_1^{(n)}(1)\right) = 0, \quad j = 1,2 \tag{29}$$

$$\sum_{j=1}^{2}\left\{(-1)^{j-1}(d-b)\mathscr{B}\frac{d\psi_j^{(n)}}{dx} + \frac{d^2\varphi_j^{(n)}}{dx^2} + t_m\frac{d^3\varphi_j^{(n)}}{dx^3}\right\}_{x=1} - M\omega_n^2\kappa^2\left.\frac{d^3\varphi_1^{(n)}}{dx^3}\right|_{x=1} = 0, \quad j = 1,2 \tag{30}$$

Kinematic boundary conditions

$$\varphi_j^{(n)}(0) = \left.\frac{d\varphi_j^{(n)}}{dx}\right|_{x=0} = \psi_j^{(n)}(0) = 0, \quad j = 1,2 \tag{31}$$

$$\left.\frac{d\varphi_1^{(n)}}{dx}\right|_{x=1} = \left.\frac{d\varphi_2^{(n)}}{dx}\right|_{x=1} \tag{32}$$

$$\psi_1^{(n)}(1) = \psi_2^{(n)}(1) + 2(d-b)\left.\frac{d\varphi_1^{(n)}}{dx}\right|_{x=1} \tag{33}$$

$$\varphi_1^{(n)}(1) = \varphi_2^{(n)}(1) \tag{34}$$

The solutions of (26) and (27) can be presented as follows

$$\varphi_j^{(n)}(x) = C_{1j}^{(n)}\cos(\beta_n x) + C_{2j}^{(n)}\sin(\beta_n x) + C_{3j}^{(n)}\cosh(\beta_n x) + C_{4j}^{(n)}\sinh(\beta_n x), \quad j = 1, 2 \tag{35}$$

$$\psi_j^{(n)}(x) = C_{5j}^{(n)}\sin(\alpha_n x) + C_{6j}^{(n)}\cos(\alpha_n x), \qquad j = 1, 2 \tag{36}$$

in which $\beta_n = \sqrt{\omega_n}$ and $\alpha_n = \omega_n/\sqrt{\mathscr{B}}$.

By utilizing (35) and (36) into the boundary conditions (28)-(34), the following system of linear algebraic equations are obtained.

$$[A(\omega_n)]_{12\times 12}\vec{C}_{12\times 12}^{(n)} = \vec{0}_{12\times 1} \tag{37}$$

In Eq. (37), $\vec{C}_{12\times 1}^{(n)}$ is defined as $\vec{C}_{12\times 1}^{(n)} = [\ C_{11}^{(n)}C_{21}^{(n)}\dots C_{61}^{(n)} \ \vdots \ C_{12}^{(n)}C_{22}^{(n)}\dots C_{62}^{(n)}\ ]^T$ where T is the transpose operator. Moreover, the nonzero elements of $[A(\omega_n)]_{12\times 12}$ are presented in Appendix A. The nontrivial solution of Eq. (37) can be found by setting the determinant of $[A]$ equal to zero. Doing so, the natural frequencies of the system are obtained. Moreover, $\vec{C}$ will be equal to the eigenvector corresponded to the zero eigenvalue of $[A]$.

In order to verify the accuracy of the presented procedure for deriving the natural frequencies and the mode-shapes, a P-flexure with geometrical and physical specifications provided in Table 1 is considered. In this table, $\hat{h}$ is the width of the flexure beams.

Table 1
Geometrical and physical specifications of the P-flexure under study.

Parameters	E	ρ	$\hat{M}$	L	$\hat{b}$	$\hat{h}$	$\hat{d}$	$\hat{t}_m$	$\hat{\kappa}$
Unit	Gpa	kg/m^3	kg	mm	mm	mm	mm	mm	mm
Value	210	7800	0.035	300	0.5	15	15	5	9.1

In Table 2, the first four natural frequencies of the system are presented. In this table, the exact findings have been compared with those of finite element simulations carried out in Abaqus and excellent agreement is observed. It has to be noted that in FE simulations, we employed the *wire* element. The stage was modeled as an elastic body with the same volumetric density and elastic modulus used for modeling the flexure beams. The connections between the beams and the stage were chosen to be *coupling*.

Table 2
Comparison of the first four frequencies of the flexure beam obtained from the proposed analytical analysis and FEA.

Mode number	1	2	3	4
Analytical (Hz)	9.7958	59.2623	66.1662	163.3500
FEA (Hz)	9.7962	59.2580	66.1700	163.3300
Error (%)	0.0041	0.0073	0.0057	0.0122

In Figs. 2-5, the first four mode-shapes of the flexure is presented. In order to make the analytical and FE modes comparable, they have been both normalized such that the vertical (for transverse modes) or axial (for axial modes) displacement

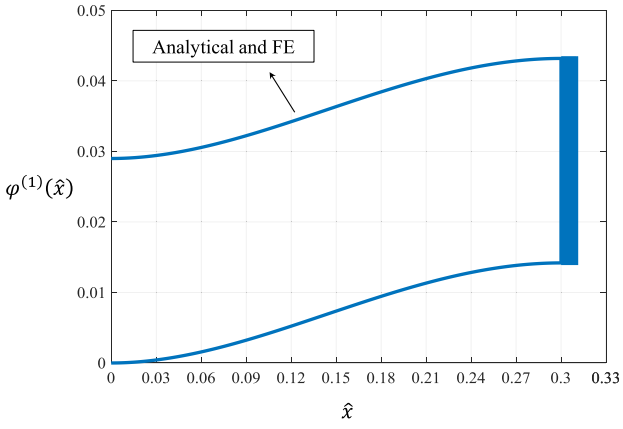

Fig. 2. First mode-shape of the system.

of the stage's center become the same for both approaches. It is readily observed that as expected, analytical modes, perfectly coincides with the numerical ones.

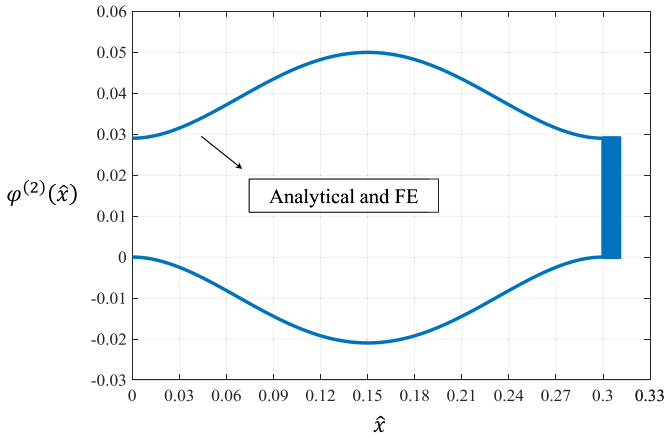

Fig. 3. Second mode-shape of the system.

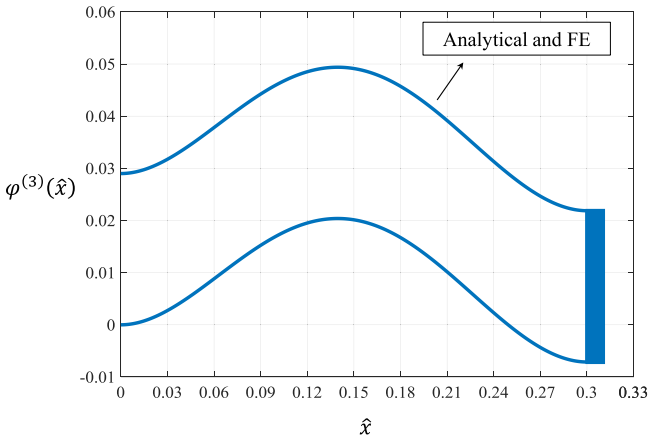

Fig. 4. Third mode-shape of the system.

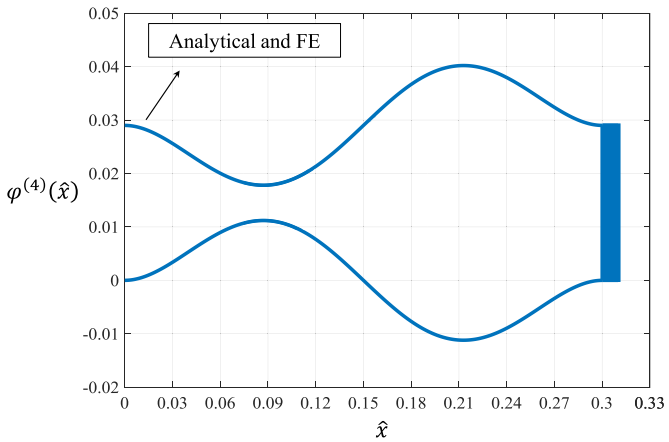

Fig. 5. Fourth mode-shape of the system.

In Fig. 6, the effects of $\hat{b}$, L, $\hat{d}$ and $\hat{M}$ on the first four natural frequencies of the P-flexure is investigated. It is observed in part (a) of this figure that with increasing $\hat{b}$, all of the natural frequencies are increased almost linearly because of the increase in the system's stiffness. Also, as depicted in Fig. 6-(b) by increasing the length of the flexure beams, the

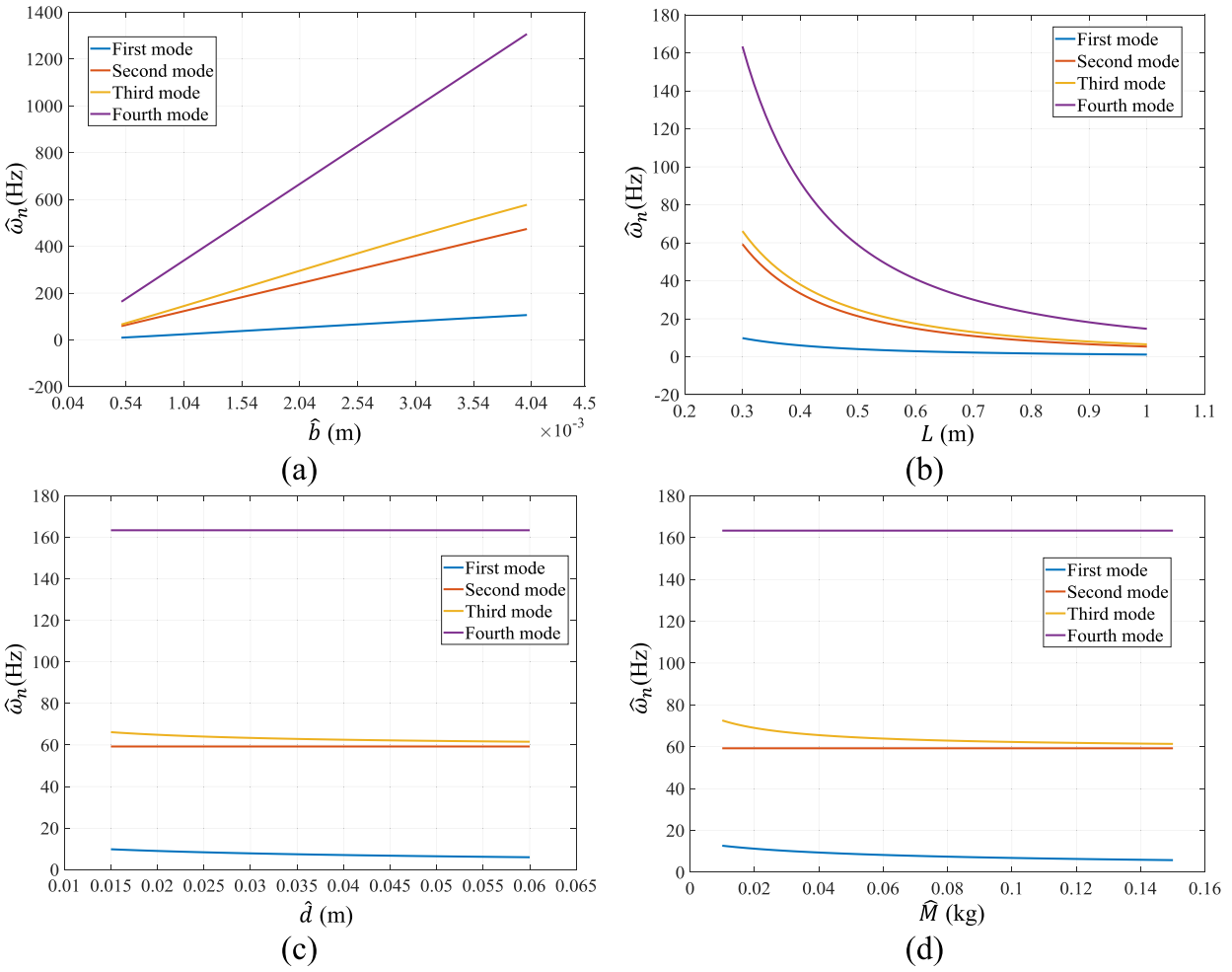

Fig. 6. The effect of (a) beam's thickness (b) beam's length (c) stage's height and (d) stage's mass on the first four natural frequencies of the P-flexure under study.

natural frequencies of the system are decreased due to the decrease in the stiffness of the system. However, at higher values of L, increasing the beams length has less effect on the natural frequencies. Fig. 6-(c) shows that by increasing $\hat{d}$ from 15mm to 60mm, the natural frequencies related to flexural modes (i.e. modes 1 and 3) experience a negligible increase (4.47×10^{-2}% for the first mode and 7.46×10^{-2}% for the third mode). However, as physically expected, those corresponded to the axial modes (i.e. modes 2 and 4) remain constant. Finally, Fig. 6-(d) reveals that by increasing the mass of the stage, the natural frequencies corresponded to the flexural modes are decreased. Nevertheless, since even in buckling modes the axial movement of the stage is very small, increasing the mass of the stage has no effect on the frequencies of the axial modes of the flexure.

4. Nonlinear analysis

In this section, we will employ the Lagrange equations along with the already derived modes to find the governing nonlinear temporal equations of motion. We will also present approximate analytical solutions for these equations.

4.1. Derivations of temporal equations of motion

We assume the dynamic response of the flexure as linear combination of its mode-shapes as

$$\hat{w}_j(\hat{x},\hat{t}) = \sum_{i=1}^{n} \varphi_j^{(i)}(\hat{x})\hat{q}_i(\hat{t}), \qquad j = 1, 2 \tag{38}$$

where n is the number of modes considered in the formulations. Moreover, in deriving the temporal equations of motion of the system, it will be more convenient to relate the tip displacements of the beams to that of the stage's center. Considering

Fig. 1 and using kinematical relationships, this can be easily achieved as

$$\hat{u}_{tip}^{(j)}(\hat{t}) = \hat{u}_{CG}(\hat{t}) + \hat{t}_m\left(1-\cos\left(\theta(\hat{t})\right)\right) + (-1)^{j-1}\left(\hat{d}-\hat{b}\right)\sin\left(\theta(\hat{t})\right),\ \ j=1,2 \tag{39}$$

$$\hat{w}_{CG}(\hat{t}) = \hat{w}_{tip}^{(j)}(\hat{t}) + \hat{t}_m\sin\left(\theta(\hat{t})\right) - \left(\hat{d}-\hat{b}\right)\left(1-\cos\left(\theta(\hat{t})\right)\right),\ \ j=1,2 \tag{40}$$

in which $\hat{u}_{tip}^{(j)}$ and $\hat{w}_{tip}^{(j)}$ are the tip axial and transversal displacements of the j'th beam respectively.

By substituting (39) (for $j=1$) and (38) into the strain energy (7), one obtains

$$\begin{aligned}\hat{\pi}\left(\hat{u}_{CG};\hat{q}_1,\hat{q}_2,\ldots,\hat{q}_n\right) = \sum_{j=1}^{2}\Bigg\{\frac{EA}{2L}\Bigg[&\hat{u}_{CG}(\hat{t}) + 2\hat{t}_m\sin^2\left(\frac{1}{2}\sum_{i=0}^{n}\left.\frac{d\varphi_j^{(i)}(\hat{x})}{d\hat{x}}\right|_{\hat{x}=L}\hat{q}_i(\hat{t})\right)\\ &(-1)^{j-1}\left(\hat{d}-\hat{b}\right)\sin\left(\frac{1}{2}\sum_{i=0}^{n}\left.\frac{d\varphi_j^{(i)}(\hat{x})}{d\hat{x}}\right|_{\hat{x}=L}\hat{q}_i(\hat{t})\right) + \frac{1}{2}\int_0^L\left(\sum_{i=0}^{n}\frac{d\varphi_j^{(i)}(\hat{x})}{d\hat{x}}\hat{q}_i(\hat{t})\right)^2 d\hat{x}\Bigg]^2\\ &+\frac{1}{2}EI\int_0^L\left(\sum_{i=0}^{n}\frac{d^2\varphi_j^{(i)}(\hat{x})}{d\hat{x}^2}\hat{q}_i(\hat{t})\right)^2 d\hat{x}\Bigg\}\end{aligned} \tag{41}$$

Also, employing (38), (39) and (40) (for $j=1$) into the kinetic energy (11) leads to

$$\begin{aligned}\hat{T}\left(\dot{\hat{u}}_{CG};\hat{q}_1,\hat{q}_2,\ldots,\hat{q}_n;\dot{\hat{q}}_1,\dot{\hat{q}}_2,\ldots,\dot{\hat{q}}_n\right) = \sum_{j=1}^{2}\Bigg\{&\frac{1}{2}\int_0^L\rho A\left(\dot{\hat{\jmath}}(t)+\sum_{i=1}^{n}\varphi_j^{(i)}(\hat{x})\dot{\hat{q}}_i(\hat{t})\right)^2 d\hat{x}\Bigg\}\\ &+\frac{1}{2}\hat{M}\dot{\hat{u}}_{CG}^2(\hat{t}) + \frac{1}{2}\hat{M}\Bigg\{\hat{t}_m\sum_{i=0}^{n}\left.\frac{d\varphi_1^{(i)}(\hat{x})}{d\hat{x}}\right|_{\hat{x}=L}\hat{q}_i(\hat{t})\cos\left(\left.\frac{d\varphi_1^{(i)}(\hat{x})}{d\hat{x}}\right|_{\hat{x}=L}\hat{q}_i(\hat{t})\right)\\ &-\left(\hat{d}-\hat{b}\right)\sum_{i=0}^{n}\left.\frac{d\varphi_1^{(i)}(\hat{x})}{d\hat{x}}\right|_{\hat{x}=L}\hat{q}_i(\hat{t})\sin\left(\left.\frac{d\varphi_1^{(i)}(\hat{x})}{d\hat{x}}\right|_{\hat{x}=L}\hat{q}_i(\hat{t})\right) + \sum_{i=1}^{n}\varphi_1^{(i)}(L)\dot{\hat{q}}_i(\hat{t})\Bigg\}^2\\ &+\frac{1}{2}\hat{M}\hat{\kappa}^2\left(\sum_{i=0}^{n}\left.\frac{d\varphi_1^{(i)}(\hat{x})}{d\hat{x}}\right|_{\hat{x}=L}\dot{\hat{q}}_i(\hat{t})\right)^2\end{aligned} \tag{42}$$

The virtual work can also be simplified by substituting (38) into (12) and (13) as

$$\delta\hat{W}_{ext}\left(\hat{u}_{CG};\hat{q}_1,\ldots,\hat{q}_n;\dot{\hat{q}}_1,\ldots,\dot{\hat{q}}_n\right) = \hat{Q}_{\hat{u}}\delta\hat{u}_{CG}(\hat{t}) + \sum_{i=1}^{n}\hat{Q}_{\hat{q}}^{(i)}\left(\hat{q}_1,\ldots,\hat{q}_n;\dot{\hat{q}}_1,\ldots,\dot{\hat{q}}_n\right)\delta\hat{q}_i(\hat{t}) \tag{43}$$

in which $\hat{Q}_{\hat{q}}^{(i)}$ and $\hat{Q}_{\hat{u}}$ are defined as

$$\hat{Q}_{\hat{q}}^{(i)}\left(\hat{q}_1,\ldots,\hat{q}_n;\dot{\hat{q}}_1,\ldots,\dot{\hat{q}}_n\right) = \hat{F}_{\hat{z}}\eta_i^{(n)}\left(\hat{q}_1,\ldots,\hat{q}_n\right) - \hat{C}\sum_{j=1}^{2}\sum_{k=1}^{n}\left(\dot{\hat{q}}_k\int_0^L\varphi_j^{(k)}(\hat{x})\varphi_j^{(i)}(\hat{x}) + 3d\hat{x}\right) \tag{44}$$

$$\hat{Q}_{\hat{u}} = \hat{F}_{\hat{x}} \tag{45}$$

In Eq. (44), the parameters $\eta_i^{(n)}(\hat{q}_1,\ldots,\hat{q}_n)$, $i=1,2$, are defined as

$$\eta_i^{(n)}\left(\hat{q}_1,\ldots,\hat{q}_n\right) = \left\{\varphi_1^{(i)}(\hat{x}) + \frac{d\varphi_1^{(i)}}{d\hat{x}}\left(\hat{t}_m\cos\left(\sum_{k=1}^{n}\frac{d\varphi_1^{(k)}}{d\hat{x}}\hat{q}_k(t)\right) - \left(\hat{d}-\hat{b}\right)\sin\left(\sum_{k=1}^{n}\frac{d\varphi_1^{(k)}}{d\hat{x}}\hat{q}_k(t)\right)\right)\right\}_{\hat{x}=L} \tag{46}$$

Using $\vec{\hat{q}} = [\hat{u}_{CG}\vdots\ \hat{q}_1\ \hat{q}_2\ldots\ \hat{q}_n]^T$ as the generalized coordinate vector in Lagrange equations, the temporal equations governing the nonlinear dynamic behavior of the system can be derived. The choice of the number of contributing modes may affect the accuracy of the analytical findings. In the following, we will proceed the formulation by considering two modes. However, we will show later that even a single mode assumption can perfectly capture almost the whole nonlinear dynamic of the system.

In order to present the nonlinear temporal equations of motion more conveniently, first, the following normalized variables are introduced.

$$q_i(t) = \frac{\hat{q}_i(\hat{t})}{L},\ u_{CG}(t) = \frac{\hat{u}_{CG}(\hat{t})}{L},\ t = \hat{t}\sqrt{\frac{\hat{M}L}{2EA}},\ F_x = \frac{\hat{F}_x L^2}{EI},\ F_z = \frac{\hat{F}_z L^2}{EI} \tag{47}$$

Using two modes assumption in the Lagrange equations, the following nonlinear normalized equations are obtained for the time domain behavior of the system.

$$u''_{CG}(t) + \sum_{j=0}^{2}\sum_{i=0}^{2}\lambda^{(1)}_{ij,1}(q_1,q_2)q_1^i(t)q_2^j(t) + u_{CG}(t) = F_x(t) \tag{48}$$

$$\begin{aligned}&\sum_{j=0}^{1}\sum_{i=0}^{1}\lambda^{(2)}_{ij,1}(q_1,q_2)q_1''^{\,i}(t)q_2''^{\,j}(t) + \sum_{j=0}^{2}\sum_{i=0}^{2}\lambda^{(2)}_{ij,2}(q_1,q_2)q_1'^{\,i}(t)q_2'^{\,j}(t)\\ &\quad+\sum_{j=0}^{3}\sum_{i=0}^{3}\lambda^{(2)}_{ij,3}(q_1,q_2)q_1^i(t)q_2^j(t) + u_{CG}(t)\sum_{j=0}^{1}\sum_{i=0}^{1}\lambda^{(2)}_{ij,4}(q_1,q_2)q_1^i(t)q_2^j(t)\\ &\quad+\lambda^{(2)}_{\mathfrak{z}}(t)\mathfrak{z}''(t) = \eta^{(2)}_1(q_1,q_2)F_z(t)\end{aligned} \tag{49}$$

$$\begin{aligned}&\sum_{j=0}^{1}\sum_{i=0}^{1}\lambda^{(3)}_{ij,1}(q_1,q_2)q_1''^{\,i}(t)q_2''^{\,j}(t) + \sum_{j=0}^{2}\sum_{i=0}^{2}\lambda^{(3)}_{ij,2}(q_1,q_2)q_1'^{\,i}(t)q_2'^{\,j}(t)\\ &\quad+\sum_{j=0}^{3}\sum_{i=0}^{3}\lambda^{(3)}_{ij,3}(q_1,q_2)q_1^i(t)q_2^j(t) + u_{CG}(t)\sum_{j=0}^{1}\sum_{i=0}^{1}\lambda^{(3)}_{ij,4}(q_1,q_2)q_1^i(t)q_2^j(t)\\ &\quad+\lambda^{(3)}_{\mathfrak{z}}(t)\mathfrak{z}''(t) = \eta^{(2)}_2(q_1,q_2)F_z(t)\end{aligned} \tag{50}$$

In these equations, the prime indicates differentiation with respect to normalized time t. The parameters $\lambda^{(l)}_{ij,k}(q_1,q_2)$ and $\lambda^{(l)}_{\mathfrak{z}}$ are some lengthy functions of system specifications as well as the generalized coordinates q_1 and q_2. The analytical formula of these parameters are provided in Appendix B.

In order to verify the accuracy of the proposed formulations, the P-flexure with specifications given in Table 1 is considered. By eliminating terms containing time derivatives in Eqs. (48)-(50), the static behavior of the system can be investigated. In Fig. 7-(a), the parameters q_1 and q_2 have been plotted versus the applied load F_z. As this figure suggests, the contribution of the second mode in the system's deflection is several orders of magnitude smaller than that of the first mode. So, consideration of the second mode in the formulations does not provide any appreciable improvement in predicting the static behavior of the system. Moreover, in Fig. 7-(b), the axial displacement of the stage's center has been depicted against its transverse one. The results of this Figure is compared with analytical findings of Awtar and Sen [23] and excellent agreement is observed.

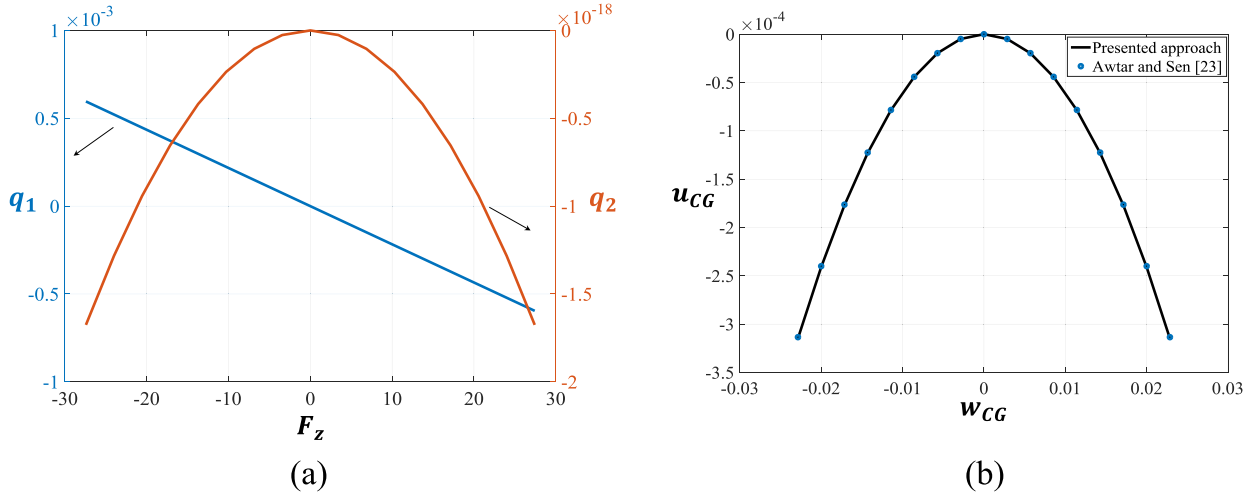

Fig. 7. (a) Generalized coordinates q_1 and q_2 versus the applied normalized force (b) Axial versus transverse displacement of the stage's center.

To make sure that the contribution of the second mode is also negligible in the dynamic response, free vibration of the system with displacement initial conditions chosen from Fig. 7-(a) (and with zero initial velocities) is simulated numerically.

Fig. 8 illustrates these dynamic responses. Comparing the values of the $q_1(t)$ and $q_2(t)$ implicitly shows that involvement of the second mode in dynamic simulations only increases the numerical effort for solving the equations of motion without any significant impact on the results. So, in the rest of this paper, the simulations will be carried out by considering only one mode.

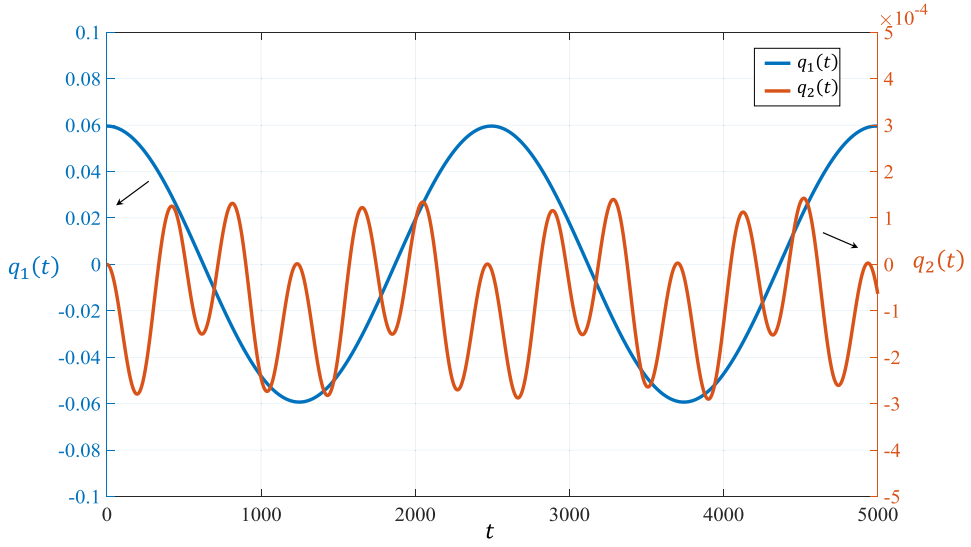

Fig. 8. Nonlinear free vibration response of the system using a two mode assumption.

By neglecting the Eq. (50) (which corresponds to the response associated with the second mode) and setting $q_2(t) = 0$ in (48) and (49), the governing dynamic equations of motion are reduced to

$$u''_{CG}(t) + \sum_{i=0}^{2} \lambda^{(1)}_{i0,1}(q_1(t), 0) q_1^i(t) + u_{CG}(t) = F_x(t) \tag{51}$$

$$\sum_{i=0}^{1} \lambda^{(2)}_{i0,1}(q_1, 0) q_1''^i(t) + \sum_{i=0}^{2} \lambda^{(2)}_{i0,2}(q_1, 0) q_1'^i(t) + \sum_{i=0}^{3} \lambda^{(2)}_{i0,3}(q_1, 0) q_1^i(t) + u_{CG}(t) \sum_{i=0}^{1} \lambda^{(2)}_{i0,4}(q_1, 0) q_1^i(t) + \lambda^{(2)}_{\jmath} \jmath''(t) = \eta^{(2)}_1(q_1, 0) F_z(t) \tag{52}$$

To solve (51) and (52) analytically using the perturbation theory, the nonlinear terms in these equations shall be replaced by their Taylor series expansion. Doing so, one gets

$$u''_{CG}(t) + \sum_{i=1}^{4} \gamma^{(1)}_{i,1} q^i(t) + u_{CG}(t) = 0 \tag{53}$$

$$\left(1 + \sum_{i=1}^{4} \gamma^{(2)}_{i,1} q^i(t)\right) q''(t) + \gamma_c q'(t) + q'^2(t) \sum_{i=0}^{4} \gamma^{(2)}_{i,2} q^i(t) + \sum_{i=1}^{6} \gamma^{(2)}_{i,3} q^i(t) + \sum_{i=0}^{4} \gamma^{(2)}_{i,4} u_{CG}(t) q^i(t) = \gamma_\jmath \sin(\Omega t) \tag{54}$$

In obtaining (54), we have also replaced the base excitation term with a harmonic function as depicted in Fig. 1. The parameters $\gamma^{(k)}_{i,j}$, γ_c and $\gamma_\jmath$ in these equations have been presented in Appendix C. Please note that for notational simplicity, in Eqs. (53) and (54), the variable q_1 has been replaced with a new variable q. Using the specifications given in Table 1, the numerical values of the coefficients appeared in Eqs. (53) and (54) (except γ_c and $\gamma_\jmath$) are compiled in Table 3. As it is observed, most of the coefficients in these equations are very small and have negligible effects on the response. In fact, one can say that the only coefficients that has impact on the nonlinear dynamic responses are $\gamma^{(1)}_{2,1}$, $\gamma^{(2)}_{1,3}$, $\gamma^{(2)}_{3,3}$ and $\gamma^{(2)}_{1,4}$. The knowledge of the order of magnitude of these coefficients will be employed in the next section along with the multiple time scales perturbation technique, to provide analytical solution for the governing temporal equations of motion.

4.2. Perturbation solution

In order to analytically model the governing Eqs. (53) and (54), the multiple time scales perturbation technique is employed. Based on this technique, the time scales $T_i = \varepsilon^i t$, $(i = 0, 1)$ are defined. The time derivatives $d(\,)/dt$ and $d^2(\,)/dt^2$ can be expanded in terms of T_is as

$$\frac{d}{dt}(\,) = \frac{\partial}{\partial T_0}(\,) + \varepsilon \frac{\partial}{\partial T_1}(\,) + O(\varepsilon^2)$$

Table 3
Value of the coefficients appeared in equations of motion (53) and (54).

Parameter	$\gamma_{1,1}^{(1)}$	$\gamma_{2,1}^{(1)}$	$\gamma_{3,1}^{(1)}$	$\gamma_{4,1}^{(1)}$
Value	-1.5583×10^{-15}	0.0887	5.2022×10^{-22}	3.0957×10^{-16}
Parameter	$\gamma_{1,1}^{(2)}$	$\gamma_{2,1}^{(2)}$	$\gamma_{3,1}^{(2)}$	$\gamma_{4,1}^{(2)}$
Value	9.5432×10^{-08}	-1.3441×10^{-11}	2.7683×10^{-14}	6.865×10^{-19}
Parameter	$\gamma_{0,2}^{(2)}$	$\gamma_{1,2}^{(2)}$	$\gamma_{2,2}^{(2)}$	$\gamma_{3,2}^{(2)}$
Value	4.7716×10^{-08}	-1.3441×10^{-11}	1.5931×10^{-14}	1.4945×10^{-18}
Parameter	$\gamma_{4,2}^{(2)}$	$\gamma_{1,3}^{(2)}$	$\gamma_{2,3}^{(2)}$	$\gamma_{3,3}^{(2)}$
Value	8.8676×10^{-22}	6.3319×10^{-06}	1.5982×10^{-15}	0.0606
Parameter	$\gamma_{4,3}^{(2)}$	$\gamma_{5,3}^{(2)}$	$\gamma_{6,3}^{(2)}$	$\gamma_{0,4}^{(2)}$
Value	8.8921×10^{-22}	-6.3498×10^{-16}	-4.9475×10^{-29}	-6.0069×10^{-15}
Parameter	$\gamma_{1,4}^{(2)}$	$\gamma_{2,4}^{(2)}$	$\gamma_{3,4}^{(2)}$	$\gamma_{4,4}^{(2)}$
Value	0.6837	6.0159×10^{-22}	-4.7732×10^{-15}	-5.5786×10^{-28}

$$\frac{d^2}{dt^2}() = \frac{\partial^2}{\partial T_0^2}() + 2\varepsilon \frac{\partial^2}{\partial T_0 \partial T_1}() + \varepsilon^2 \frac{\partial^2}{\partial T_1^2}() + O(\varepsilon^3) \tag{55}$$

A physical understanding of the system reveals that the deflection of the flexure beams is one order of magnitude smaller than their length. Moreover, it is also observed that the axial displacements are one order of magnitude smaller than that of the transverse ones. So, by considering the normalization scheme presented in Eq. (47), one can say

$$q(t) \approx O(\varepsilon), \quad u_{CG}(t) \approx O(\varepsilon^2) \tag{56}$$

Using Eq. (56), the perturbation expansion of q and u_{CG} is expressed as

$$q(T_0, T_1) = \varepsilon(\mathrm{q}_0(T_0, T_1) + \varepsilon \mathrm{q}_1(T_0, T_1)) \tag{57}$$

$$u_{CG}(T_0, T_1) = \varepsilon^2(u_{CG,0}(T_0, T_1) + \varepsilon u_{CG,1}(T_0, T_1)) \tag{58}$$

Considering the order of magnitude of the coefficients given in Table 3, it is assumed that

$$O(\gamma_{i,j}^{(k)}) = \varepsilon^k, \ \ k \geq 3, \ \ \gamma_{i,j}^{(k)} \notin \{\gamma_{2,1}^{(1)}, \ \gamma_{3,3}^{(2)}, \ \gamma_{1,4}^{(2)}, \gamma_{1,3}^{(2)}\} \tag{59}$$

Furthermore, the damping coefficient which reflects the modal damping of the first mode is supposed to be small. So, we use the following scaling scheme for γ_c.

$$\gamma_c = \varepsilon \bar{\gamma}_c \tag{60}$$

4.2.1. Nonlinear free vibration analysis

In the case of the free vibration, the excitation term (i.e.γ_3) can be dropped. Moreover, by substituting (55) and (57)-(60) into (53) and (54), while collecting like powers of ε, the following equations are obtained.

$$\begin{cases} \dfrac{\partial^2 \mathrm{q}_0(T_0, T_1)}{\partial T_0^2} + \gamma_{1,3}^{(2)} \mathrm{q}_0(T_0, T_1) = 0 \end{cases} \tag{61}$$

$$\begin{cases} \dfrac{\partial^2 \mathrm{q}_1(T_0, T_1)}{\partial T_0^2} + \gamma_{1,3}^{(2)} \mathrm{q}_1(T_0, T_1) = -2\dfrac{\partial^2 \mathrm{q}_0(T_0, T_1)}{\partial T_0 \partial T_1} - \overline{\gamma}_c \dfrac{\partial \mathrm{q}_0(T_0, T_1)}{\partial T_0} \end{cases} \tag{62}$$

$$\begin{cases} \dfrac{\partial^2 u_{CG,0}(T_0, T_1)}{\partial T_0^2} + u_{CG,0}(T_0, T_1) = -\gamma_{2,1}^{(1)} \mathrm{q}_0^2(T_0, T_1) \end{cases} \tag{63}$$

$$\begin{cases} \dfrac{\partial^2 u_{CG,1}(T_0, T_1)}{\partial T_0^2} + u_{CG,1}(T_0, T_1) = -2\dfrac{\partial^2 u_{CG,0}(T_0, T_1)}{\partial T_0 \partial T_1} - 2\gamma_{2,1}^{(1)} \mathrm{q}_0(T_0, T_1) \mathrm{q}_1(T_0, T_1) \end{cases} \tag{64}$$

The solution of (61) is as

$$\mathrm{q}_0(T_0, T_1) = \mathbb{A}(T_1) \exp\left(I\sqrt{\gamma_{1,3}^{(2)}} T_0\right) + cc \tag{65}$$

in which $\mathbb{A}$ is a complex function of T_1 and cc denotes the complex conjugate of all of the proceeding terms. By substituting (65) into (63) and solving the outcome, the response associated with $u_{CG,\,0}$ is derived as

$$u_{CG,0}(T_0, T_1) = \mathbb{B}(T_1) \exp(IT_0) + \frac{1}{4\gamma_{1,3}^{(2)} - 1} \gamma_{2,1}^{(1)} \mathbb{A}^2(T_1) \exp\left(2I\sqrt{\gamma_{1,3}^{(2)}} T_0\right) - 2\gamma_{2,1}^{(1)} \mathbb{A}(T_1) \bar{\mathbb{A}}(T_1) + cc \tag{66}$$

where $\mathbb{B}$ is an unknown complex function which will be determined by eliminating secular terms from the response of (64). Furthermore, by substituting (65) in (62) and performing some mathematical simplifications, one gets

$$\frac{\partial^2 \mathfrak{q}_1(T_0,T_1)}{\partial T_0^2}+\gamma_{1,3}^{(2)}\mathfrak{q}_1(T_0,T_1)=-I\sqrt{\gamma_{1,3}^{(2)}}\left(2\frac{d\mathbb{A}(T_1)}{dT_1}+\overline{\gamma}_c\mathbb{A}(T_1)\right)\exp\left(I\sqrt{\gamma_{1,3}^{(2)}}T_0\right)+cc \tag{67}$$

Any solution of (67) will contain a secular term unless the coefficient of $\exp(I\sqrt{\gamma_{1,3}^{(2)}}T_0)$ in the right-hand side of this equation becomes zero. So, to remove secular terms, we assume

$$2\frac{d\mathbb{A}(T_1)}{dT_1}+\bar{\gamma}_c\mathbb{A}(T_1)=0 \tag{68}$$

To solve this equation, $\mathbb{A}(T_1)$ is expressed in polar form as

$$\mathbb{A}(T_1)=\frac{1}{2}\mathfrak{a}(T_1)\exp\left(I\phi(T_1)\right) \tag{69}$$

By substituting (69) into (68) and separating the real and imaginary parts, it is concluded that

$$\frac{d\mathfrak{a}(T_1)}{dT_1}+\frac{1}{2}\bar{\gamma}_c\mathfrak{a}(T_1)=0 \tag{70}$$

$$\mathfrak{a}(T_1)\frac{d\phi(T_1)}{dT_1}=0 \tag{71}$$

The solution of these equations can be easily found as

$$\mathfrak{a}(T_1)=\mathfrak{a}_0\exp\left(-\frac{1}{2}\bar{\gamma}_cT_1\right) \tag{72}$$

$$\phi(T_1)=\phi_0 \tag{73}$$

Now by putting (72) and (73) into (69) and employing the outcome into (65)-(67), $\mathfrak{q}_0(T_0,T_1)$, $u_{CG,0}(T_0,T_1)$ and the particular solution of $\mathfrak{q}_1(T_0,T_1)$ are derived as

$$\mathfrak{q}_0(T_0,T_1)=\frac{1}{2}\mathfrak{a}_0\exp\left(-\frac{1}{2}\bar{\gamma}_cT_1\right)\exp\left(I\sqrt{\gamma_{1,3}^{(2)}}T_0+I\phi_0\right)+cc \tag{74}$$

$$u_{CG,0}(T_0,T_1)=\mathbb{B}(T_1)\exp\left(IT_0\right)+\left\{\exp\left(\left(4\sqrt{\gamma_{1,3}^{(2)}}T_0+2\phi_0\right)I\right)-2\left(4\gamma_{1,3}^{(2)}-1\right)\right\}\times\frac{\mathfrak{a}^2\gamma_{2,1}^{(1)}\exp\left(-\bar{\gamma}_cT_1\right)}{4\left(4\gamma_{1,3}^{(2)}-1\right)}+cc \tag{75}$$

$$\mathfrak{q}_1(T_0,T_1)=0 \tag{76}$$

Now by employing (74)-(76), Eq. (64) is simplified as

$$\frac{\partial^2 u_{CG,1}(T_0,T_1)}{\partial T_0^2}+u_{CG,1}(T_0,T_1)=2I\,\frac{d\mathbb{B}(T_1)}{dT_1}\exp\left(IT_0\right)-2I\frac{\bar{\gamma}_c\gamma_{2,1}^{(1)}\sqrt{\gamma_{1,3}^{(2)}}}{4\gamma_{1,3}^{(2)}-1}\mathfrak{a}_0^2$$
$$\times\exp\left(-\bar{\gamma}_cT_1+2I\left(2\sqrt{\gamma_{1,3}^{(2)}}T_0+\phi_0\right)\right)+cc \tag{77}$$

To avoid secular terms in response of (77), the coefficients of $\exp(IT_0)$ in this equation has to be set to zero.

$$\frac{d\mathbb{B}(T_1)}{dT_1}=0 \tag{78}$$

Assuming the following polar form for $\mathbb{B}(T_1)$,

$$\mathbb{B}(T_1)=\frac{1}{2}\mathbb{b}(T_1)\exp\left(I\vartheta(T_1)\right) \tag{79}$$

substituting it in (78) and separating the real and imaginary parts of the resulting equation, leads to

$$\frac{d\mathbb{b}(T_1)}{dT_1}=0 \tag{80}$$

$$\mathbb{b}(T_1)\frac{d\vartheta(T_1)}{dT_1}=0 \tag{81}$$

The solution of (80) and (81) are respectively $\mathbb{b}(T_1)=\mathbb{b}_0$ and $\vartheta(T_1)=\vartheta_0$ which upon substitution in (79), results in

$$\mathbb{B}(T_1)=\frac{1}{2}\mathbb{b}_0\exp\left(I\vartheta_0\right) \tag{82}$$

Now by substituting (69) and (82) into (66) along with considering (72) and (73), $u_{CG,0}(T_0, T_1)$ is found as

$$u_{CG,0}(T_0,T_1)=\frac{1}{2}\mathbb{b}_0\exp\left(I(T_0+\vartheta_0)\right)+\left(\exp\left(4I\sqrt{\gamma_{1,3}^{(2)}}+2I\phi_0\right)-8\gamma_{1,3}^{(2)}+2\right)\times\frac{\gamma_{2,1}^{(1)}\mathbb{a}_0^2\exp\left(\bar{\gamma}_c T_1\right)}{4\left(4\gamma_{1,3}^{(2)}-1\right)}+cc \tag{83}$$

Finally, by considering Eqs. (74) and (83), the transverse and axial dynamic of the P-flexure up to the zeroth order perturbation expansion are reduced to

$$q(t)=\frac{1}{2}\mathbb{a}\exp\left(-\frac{1}{2}\gamma_c t\right)\cos\left(\sqrt{\gamma_{1,3}^{(2)}}t+\phi_0\right) \tag{84}$$

$$u_{CG}(t)=\mathbb{b}\cos\left(t+\vartheta_0\right)-\frac{\gamma_{2,1}^{(1)}\mathbb{a}^2}{2-8\gamma_{1,3}^{(2)}}\exp\left(-\gamma_c t\right)\left(1+\cos\left(2\left(\sqrt{\gamma_{1,3}^{(2)}}t+\phi_0\right)\right)\right) \tag{85}$$

in which $\mathbb{a}=\varepsilon\mathbb{a}_0$, $\mathbb{b}=\varepsilon^2\mathbb{b}_0$.

To examine the accuracy of the proposed analytical closed-form expressions, again, the P-flexure with specifications given in Table 1 with zero damping coefficient is considered. The initial velocities are set to zero and the initial displacements are selected from the static deflection curve given in Fig. 7-(b). In Figs. 9-(a) and (b), the free transverse and axial vibration response of this system are illustrated respectively. It is observed that the results of the presented analytical technique matches perfectly with those obtained from numerical calculations. The phase plane plots of $q(t)$ and $u_{CG}(t)$ are also depicted respectively in parts (c) and (d) of this figure. The latter clearly reveals that the axial dynamic contains high frequency low amplitude oscillations (originated from high axial elastic stiffness) as well as a low frequency high amplitude one (resulted from elasto-kinematic effects).

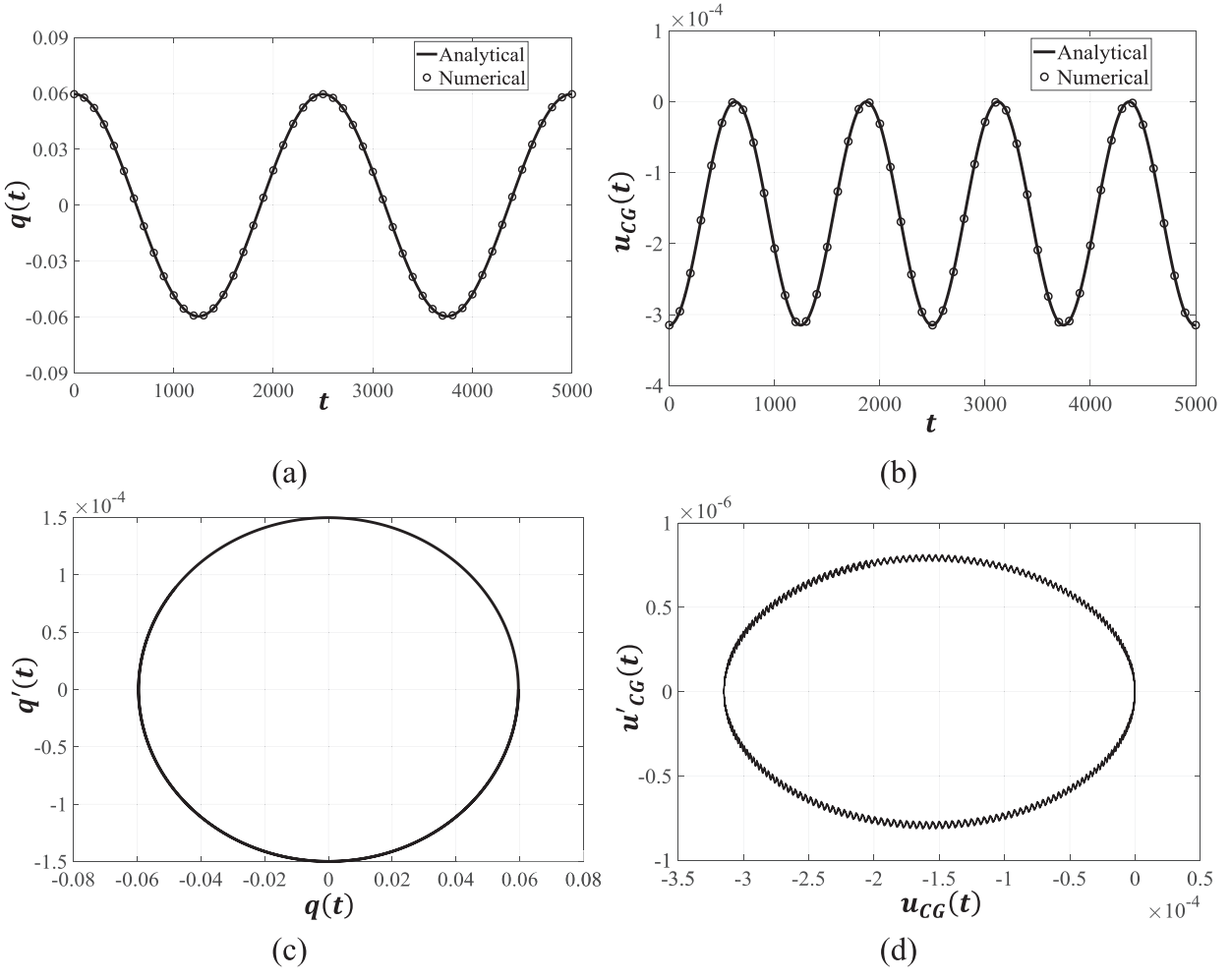

Fig. 9. Free vibration response of the un-damped P-flexure (a) transverse and (b) axial time history response (c) phase plane of the transverse and (d) axial response.

Fig. 10 shows the same results for the damped system with a nominal dimensionless damping value of $\gamma_c = 7.562 \times 10^{-4}$ (corresponded to $\hat{C} = 5\ Ns/m$). It is again observed that the results are in good agreement. But this time, the analytical and numerical findings of the transverse and axial vibration frequencies have 1.30% and 1.42% discrepancies.

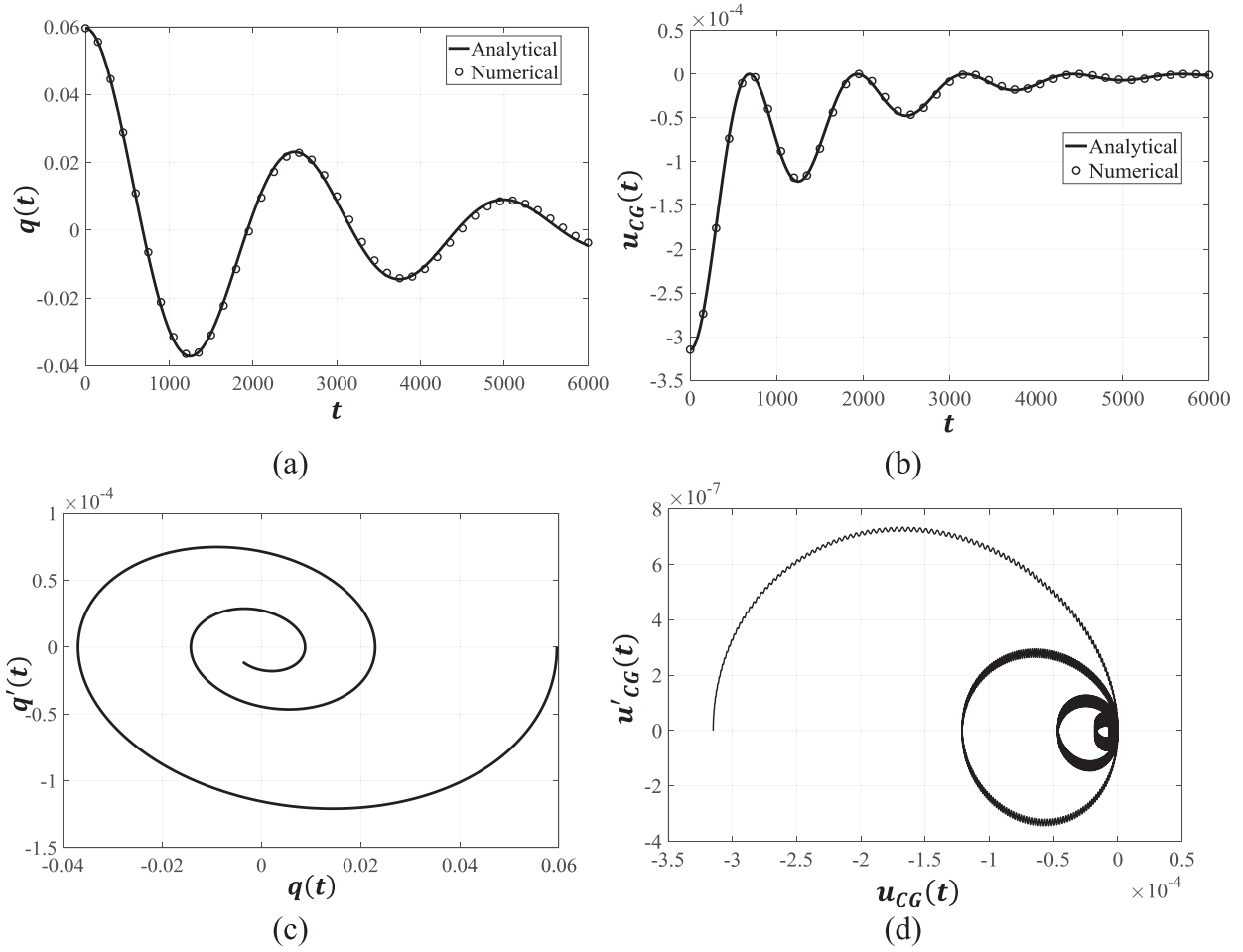

Fig. 10. Free vibration response of the damped P flexure with $\gamma_c = 7.562 \times 10^{-4}$ (a) Transverse response (b) axial response (c) phase plane results of the transverse response (d) phase plane results of the axial response.

Fig. 11 shows the dynamic trajectory of the center of gravity of the stage using two different horizontal axes on the top and the bottom. The curve corresponded to the latter, presents the details of the planar motion trajectory, while the one related to the former, verifies that even in the dynamic state, the error motion in P flexures is very small and the resulted guided motion is almost a straight line.

4.2.2. Near resonance response

The forced vibration analysis of the P-flexure under harmonic base movements will be analyzed in this section. A possible application for this case is energy harvesting from vibrating environments. In energy scavenging devices, it is usually tried to set the resonant frequency of the system to the excitation frequency of the media [49]. This, results in greater displacements of the motion stage which in turn would be accompanied by more harvested power. Considering these points, we will only analyze the forced vibration of the system in the near resonant state. Comparing to the free vibration case, we will start the perturbation expansions from a lower power of ε to account for larger displacements resulted from near resonance excitation. So, one can say

$$q(T_0, T_1) = \mathrm{q}_0(T_0, T_1) + \varepsilon \mathrm{q}_1(T_0, T_1) \tag{86}$$

$$u_{CG}(T_0, T_1) = \varepsilon u_{CG,0}(T_0, T_1) + \varepsilon^2 u_{CG,1}(T_0, T_1) \tag{87}$$

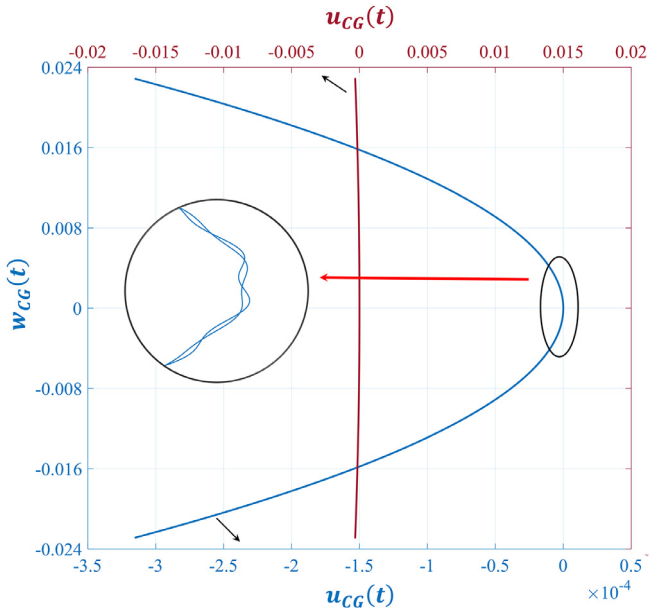

Fig. 11. Planar dynamic trajectory of the center of gravity of the stage.

Since as given in Appendix C, γ_3 is some coefficient of $\hat{\mathbb{Z}}_b/L$ (which is $O(\varepsilon)$), one can assume that the flexure is under soft excitation.

$$\gamma_3 = \varepsilon\bar{\gamma}_3 \tag{88}$$

Also, to seek for mathematical simplicity and by considering Table 3, we employ the following scaling factors for some of the coefficients of the differential Eq. (54).

$$\gamma_{3,3}^{(2)} = \varepsilon\bar{\gamma}_{3,3}^{(2)},\ \ \gamma_{1,4}^{(2)} = \varepsilon\bar{\gamma}_{1,4}^{(2)} \tag{89}$$

Now, by substituting Eqs. (55), (59), (60) and (86)-(89) into (53) and (54), while collecting the coefficients of the like powers of ε, one gets

$$\begin{cases} \dfrac{\partial^2 q_0(T_0,T_1)}{\partial T_0^2} + \gamma_{1,3}^{(2)} q_0(T_0,T_1) = 0 & (90) \\ \dfrac{\partial^2 q_1(T_0,T_1)}{\partial T_0^2} + \gamma_{1,3}^{(2)} q_1(T_0,T_1) = -2\dfrac{\partial^2 q_0(T_0,T_1)}{\partial T_0 \partial T_1} - \overline{\gamma}_c \dfrac{\partial q_0(T_0,T_1)}{\partial T_0} - \overline{\gamma}_{3,3}^{(2)} q_0^3(T_0,T_1) + \overline{\gamma}_3 \sin(\Omega T_0) & (91) \end{cases}$$

$$\begin{cases} \dfrac{\partial^2 u_{CG,0}(T_0,T_1)}{\partial T_0^2} + u_{CG,0}(T_0,T_1) = -2\gamma_{2,1}^{(1)} q_0(T_0,T_1) q_1(T_0,T_1) & (92) \\ \dfrac{\partial^2 u_{CG,1}(T_0,T_1)}{\partial T_0^2} + u_{CG,1}(T_0,T_1) = -2\dfrac{\partial^2 u_{CG,0}(T_0,T_1)}{\partial T_0 \partial T_1} - \gamma_{2,1}^{(1)} q_1^2(T_0,T_1) & (93) \end{cases}$$

The solution of the Eq. (90) is as already been given in (65). So, by substituting (65) into (91), it is converted to

$$\begin{aligned} \frac{\partial^2 q_1(T_0,T_1)}{\partial T_0^2} + \gamma_{1,3}^{(2)} q_1(T_0,T_1) = & -I\bar{\gamma}_c \mathbb{A}(T_1)\sqrt{\gamma_{1,3}^{(2)}} \exp\left(I\sqrt{\gamma_{1,3}^{(2)}}T_0\right) \\ & -(\mathbb{A}(T_1))^3 \bar{\gamma}_{3,3}^{(2)} \exp\left(3I\sqrt{\gamma_{1,3}^{(2)}}T_0\right) - 3\mathbb{A}(T_1)\left(\bar{\mathbb{A}}(T_1)\right)^2 \bar{\gamma}_{3,3}^{(2)} \exp\left(I\sqrt{\gamma_{1,3}^{(2)}}T_0\right) - 2I\frac{d\mathbb{A}(T_1)}{dT_1}\sqrt{\gamma_{1,3}^{(2)}} \exp\left(I\sqrt{\gamma_{1,3}^{(2)}}T_0\right) \\ & -\frac{1}{2}I\bar{\gamma}_3 \exp(I\Omega T_0) + cc \end{aligned} \tag{94}$$

Since the system is excited in near resonance state, it is reasonable to assume $\Omega \approx \sqrt{\gamma_{1,3}^{(2)}}$. On the other hand, the terms containing $\exp(I\sqrt{\gamma_{1,3}^{(2)}}T_0)$, can produce secular terms in response of (94). To investigate the near resonance response, it is assumed that

$$\Omega = \sqrt{\gamma_{1,3}^{(2)}} + \varepsilon\sigma \tag{95}$$

where σ is called the detuning parameter. Consequently, we can conclude

$$\exp(I\Omega T_0) = \exp(\sigma T_1)\exp\left(I\sqrt{\gamma_{1,3}^{(2)}}T_0\right) \tag{96}$$

By substituting (69) and (96) into the right hand side of (94), setting the coefficients of the terms capable of producing secular response to zero and performing some mathematical manipulations, the following equation is obtained.

$$\frac{1}{2}I\bar{\gamma}_c a(T_1)\sqrt{\gamma_{1,3}^{(2)}} + \frac{3}{8}\bar{\gamma}_{3,3}^{(2)}a^3(T_1) + I\sqrt{\gamma_{1,3}^{(2)}}\frac{da(T_1)}{dT_1} - \sqrt{\gamma_{1,3}^{(2)}}a(T_1)\frac{d\phi(T_1)}{dT_1} + \frac{1}{2}I\bar{\gamma}_\jmath \exp(I(\sigma T_1 - \phi(T_1))) = 0 \tag{97}$$

Separating the real and imaginary parts of (97), leads to

$$\frac{3}{8}\bar{\gamma}_{3,3}^{(2)}a^3(T_1) - \sqrt{\gamma_{1,3}^{(2)}}a(T_1)\frac{d\phi(T_1)}{dT_1} = \frac{1}{2}\bar{\gamma}_\jmath \sin(\mathrm{Y}(T_1)) \tag{98}$$

$$\left(\frac{1}{2}\bar{\gamma}_c a(T_1) + \frac{da(T_1)}{dT_1}\right) \times \sqrt{\gamma_{1,3}^{(2)}} = -\frac{1}{2}\bar{\gamma}_\jmath \cos(\mathrm{Y}(T_1)) \tag{99}$$

in which

$$\mathrm{Y}(T_1) = \sigma T_1 - \phi(T_1) \tag{100}$$

Using (100), the non-autonomous Eq. (98) can be transformed to the following autonomous equation.

$$\frac{3}{8}\bar{\gamma}_{3,3}^{(2)}a^3(T_1) - \sqrt{\gamma_{1,3}^{(2)}}a(T_1)\left(\sigma - \frac{d\mathrm{Y}(T_1)}{dT_1}\right) = \frac{1}{2}\bar{\gamma}_\jmath \sin \mathrm{Y}(T_1) \tag{101}$$

In the steady-state, the dependence of $a(T_1)$ and $\mathrm{Y}(T_1)$ to T_1 vanishes. So, by squaring both sides of (101) and (99) and adding the outcomes, while noting (88) and (89), the nonlinear frequency response of the system is obtained as

$$\left(\frac{9}{16}\left(\gamma_{3,3}^{(2)}\right)^2\right)a^6(T_1) - \left(3\varepsilon\sigma\gamma_{3,3}^{(2)}\sqrt{\gamma_{1,3}^{(2)}}\right)a^4(T_1) + \left(\gamma_{1,3}^{(2)}\left(4(\varepsilon\sigma)^2 + \gamma_c^2\right)\right) \times a^2(T_1) = \gamma_\jmath^2 \tag{102}$$

This frequency response has been plotted in Fig. 12 for different normalized damping coefficients. It is observed that as expected, with increasing the damping, the maximum amplitude of the nonlinear response is decreased. More importantly, this figure shows that although the frequency at which the maximum amplitude occurs, may not happen at $\Omega = \sqrt{\gamma_{1,3}^{(2)}}$ (i.e. the frequency of the linearized system as mentioned in (95)), unstable zones does not exist in the dynamic response. In other words, smooth variations of the excitation frequency would not lead to discontinuous changes in the vibrational amplitude.

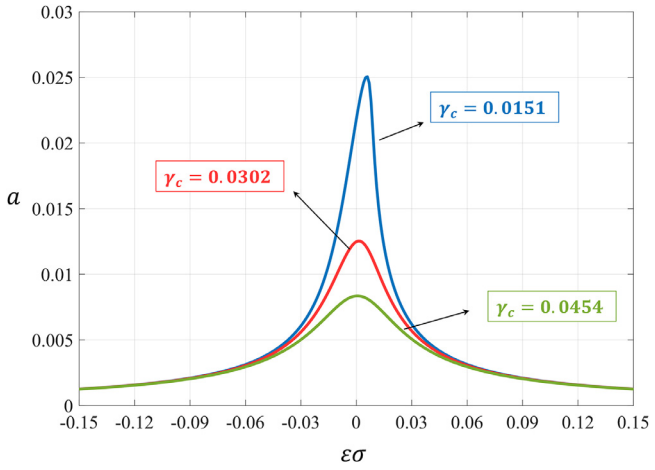

Fig. 12. Frequency response of the system for different value of damping coefficient.

5. Conclusion

The importance of accurate dynamic modeling and simulation of flexure mechanisms are well-recognized. Due to the geometric nonlinearities arisen from the large displacements, the constraint behavior of the compliant units and employment of multi bodies in their structure, such a dynamic modeling is not convenient and trivial. So, the aim of the current research was to develop a nonlinear dynamic distributed parameter formulation for a P-flexure. The governing equations were derived based on the Hamilton's principle. Various static and dynamic simulations were performed to verify

the accuracy of the proposed model and determine the number of contributing modes on the dynamic response. The nonlinear free and forced vibration responses of the system are then analyzed using the multiple time scales perturbation technique. The axial and transversal responses of the system were then validated by comparing them with numerical simulations.

As mentioned earlier, flexure mechanisms are well-suited for applications which requires large range, high precision and high-speed movements. So, derivation of a dynamic model is an essential step in their design. In the current paper, we provided a dynamic model for a simple P-flexure. This work can be continued by employing the same approach for dynamic modeling of more complex and more practical compliant units such as DP and DP-DP flexure modules.

Appendix A. Nonzero elements of [*A*]

The non-zero elements of the matrix [*A*] used for finding the natural frequencies of the system are as follows.

$$a_{1,1} = a_{1,3} = a_{2,2} = a_{2,4} = a_{3,6} = a_{4,7} = a_{4,9} = a_{5,8} = a_{5,10} = a_{6,12} = 1 \tag{A-1}$$

$$a_{7,1} = -\omega_n^2\beta_n(d-b)\sin(\beta_n),\quad a_{7,2} = \omega_n^2\beta_n(d-b)\cos(\beta_n)$$
$$a_{7,3} = \omega_n^2\beta_n(d-b)\sinh(\beta_n),\quad a_{7,4} = \omega_n^2\beta_n(d-b)\cosh(\beta_n)$$
$$a_{7,5} = -\omega_n^2\sin(\alpha_n) + (\mathscr{B}/M)\alpha_n\cos(\alpha_n),\quad a_{7,6} = -\omega_n^2\cos(\alpha_n) - (\mathscr{B}/M)\alpha_n\sin(\alpha_n) \tag{A-2}$$
$$a_{7,11} = (\mathscr{B}/M)\alpha_n\cos(\alpha_n),\qquad a_{7,12} = -(\mathscr{B}/M)\alpha_n\sin(\alpha_n)$$

$$a_{8,1} = -\beta_n^3\sin(\beta_n) - M\omega_n^2\cos(\beta_n) + M\omega_n^2 t_m\beta_n\sin(\beta_n)$$
$$a_{8,2} = \beta_n^3\cos(\beta_n) - M\omega_n^2\sin(\beta) - M\omega_n^2 t_m\beta_n\cos(\beta_n)$$
$$a_{8,3} = -\beta_n^3\sinh(\beta_n) - M\omega_n^2\cosh(\beta_n) - M\omega_n^2 t_m\beta_n\sinh(\beta_n) \tag{A-3}$$
$$a_{8,4} = -\beta_n^3\cosh(\beta_n) - M\omega_n^2\sinh(\beta_n) - M\omega_n^2 t_m\beta_n\cosh(\beta_n)$$
$$a_{8,7} = -\beta_n^3\sin(\beta_n),\ a_{8,8} = \beta_n^3\cos(\beta_n)$$
$$a_{8,9} = \beta_n^3\sinh(\beta_n),\ a_{8,10} = \beta_n^3\cosh(\beta_n)$$

$$a_{9,1} = -\beta_n^2\cos(\beta_n) + t_m\beta_n^3\sin(\beta_n) + M\omega_n^2\kappa^2\beta_n\sin(\beta_n)$$
$$a_{9,2} = -\beta_n^2\sin(\beta_n) - t_m\beta_n^3\cos(\beta_n) - M\omega_n^2\kappa^2\beta_n\cos(\beta_n)$$
$$a_{9,3} = \beta_n^2\cosh(\beta_n) + t_m\beta_n^3\sinh(\beta_n) - M\omega_n^2\kappa^2\beta_n\sinh(\beta_n)$$
$$a_{9,4} = \beta_n^2\sinh(\beta_n) + t_m\beta_n^3\cosh(\beta_n) - M\omega_n^2\kappa^2\beta_n\cosh(\beta_n)$$
$$a_{9,5} = \mathscr{B}(d-b)\alpha_n\cos(\alpha_n),\quad a_{9,6} = -\mathscr{B}(d-b)\alpha_n\sin(\alpha_n) \tag{A-4}$$
$$a_{9,7} = -\beta_n^2\cos(\beta_n) + t_m\beta_n^3\sin(\beta_n)$$
$$a_{9,8} = -\beta_n^2\sin(\beta_n) - t_m\beta_n^3\cos(\beta_n)$$
$$a_{9,9} = \beta_n^2\cosh(\beta_n) + t_m\beta_n^3\sinh(\beta_n)$$
$$a_{9,10} = \beta_n^2\sinh(\beta_n) + t_m\beta_n^3\cosh(\beta_n)$$
$$a_{9,11} = -\mathscr{B}(d-b)\alpha_n\cos(\alpha_n),\quad a_{9,12} = \mathscr{B}(d-b)\alpha_n\sin(\alpha_n)$$

$$a_{10,1} = 2\beta_n(d-b)\sin(\beta_n),\quad a_{10,2} = -2\beta_n(d-b)\cos(\beta_n)$$
$$a_{10,4} = -2\beta_n(d-b)cosh(\beta_n),\quad a_{10,3} = -2\beta_n(d-b)\sinh(\beta_n) \tag{A-5}$$
$$a_{10,5} = sin(\alpha_n),\quad a_{10,6} = cos(\alpha_n)$$
$$a_{10,11} = -\sin(\alpha_n),\quad a_{10,12} = -\cos(\alpha_n)$$

$$a_{11,1} = \cos(\beta_n),\quad a_{11,2} = \sin(\beta_n),\quad a_{11,3} = \cosh(\beta_n),\quad a_{11,4} = \sinh(\beta_n) \tag{A-6}$$
$$a_{11,7} = -\cos(\beta_n),\quad a_{11,8} = -\sin(\beta_n),\quad a_{11,9} = -\cosh(\beta_n),\quad a_{11,10} = -\sinh(\beta_n)$$

$$a_{12,1} = -\beta_n\sin(\beta_n),\quad a_{12,2} = \beta_n\cos(\beta_n),\quad a_{12,3} = \beta_n\sinh(\beta_n),$$
$$a_{12,4} = \beta_n\cosh(\beta_n),\ a_{12,7} = \beta_n\sin(\beta_n),\ a_{12,8} = -\beta_n\cos(\beta_n), \tag{A-7}$$
$$a_{12,9} = -\beta_n\sinh(\beta_n),\ a_{12,10} = -\beta_n\cosh(\beta_n)$$

Appendix B. Definition of the coefficients $\lambda_{ij,k}^{(l)}(q_1, q_2)$ and $\lambda_{j}^{(l)}$

In order to present the coefficients $\lambda_{ij,k}^{(l)}(q_1, q_2)$ and $\lambda_{j}^{(l)}$ appeared in Eqs. (48)-(50) more conveniently, we first need to define the following functions.

$$\mathfrak{F}_{j,\ 1}(\varrho) = \sin\left(\varrho\sum_{i=1}^{2}\frac{d\varphi_j^{(i)}}{dx}\bigg|_{x=1} q_i(t)\right)$$

$$\mathfrak{F}_{j,\ 2}(\varrho) = \cos\left(\varrho \sum_{i=1}^{2} \left.\frac{d\varphi_j^{(i)}}{dx}\right|_{x=1} q_i(t)\right) \tag{B-1}$$

Now, the intermediate parameters $\alpha_i^{(j)}$s are defined as

$$\alpha_1^{(1)} = \hat{M} \tag{B-2}$$

$$\alpha_2^{(1)} = \frac{EA}{2}\sum_{j=1}^{2}\int_0^1 \left(\frac{d\varphi_j^{(1)}(x)}{dx}\right)^2 dx \tag{B-3}$$

$$\alpha_3^{(1)} = \frac{EA}{2}\sum_{j=1}^{2}\int_0^1 \left(\frac{d\varphi_j^{(2)}(x)}{dx}\right)^2 dx \tag{B-4}$$

$$\alpha_4^{(1)} = EA\sum_{j=1}^{2}\int_0^1 \prod_{i=1}^{2}\frac{d\varphi_j^{(i)}(x)}{dx}dx \tag{B-5}$$

$$\alpha_5^{(1)} = 2EA \tag{B-6}$$

$$\alpha_6^{(1)} = EA\sum_{j=1}^{2}\left(2t_m\mathfrak{F}_{j,\ 1}^2(0.5) + (-1)^{j-1}(d-b)\mathfrak{F}_{j,\ 1}(1)\right) \tag{B-7}$$

$$\begin{aligned}\alpha_1^{(2)} = {} & \rho AL\sum_{j=1}^{2}\int_0^1 \left(\varphi_j^{(1)}(x)\right)^2 dx + \hat{M}\Bigg\{\left(\varphi_1^{(1)}(x)\right)^2 + \kappa^2\left(\frac{d\varphi_1^{(1)}(x)}{dx}\right)^2 \\ & + \left(\frac{d\varphi_1^{(1)}(x)}{dx}\right)^2\left((d-b)^2\mathfrak{F}_{1,\ 1}^2(1) + t_m^2\mathfrak{F}_{1,\ 2}^2(1)\right) - 2\varphi_1^{(1)}(x)\left(\frac{d\varphi_1^{(1)}(x)}{dx}\right) \\ & \times\left((d-b)\mathfrak{F}_{1,\ 1}(1) - t_m\mathfrak{F}_{1,\ 2}(1)\right) - t_m(d-b)\left(\frac{d\varphi_1^{(1)}(x)}{dx}\right)^2\mathfrak{F}_{1,\ 1}(2)\Bigg\}_{x=1}\end{aligned} \tag{B-8}$$

$$\begin{aligned}\alpha_2^{(2)} = {} & \rho AL\sum_{j=1}^{2}\int_0^1 \varphi_j^{(1)}(x)\varphi_j^{(2)}(x)dx + \hat{M}\Bigg\{\varphi_1^{(1)}(x)\varphi_1^{(2)}(x) + \kappa^2\prod_{i=1}^{2}\frac{d\varphi_1^{(i)}(x)}{dx} \\ & + \prod_{i=1}^{2}\frac{d\varphi_1^{(i)}(x)}{dx}\left((d-b)^2\mathfrak{F}_{1,\ 1}^2(1) + t_m^2\mathfrak{F}_{1,\ 2}^2(1)\right) - \frac{d}{dx}\left(\varphi_1^{(1)}(x)\varphi_1^{(2)}(x)\right) \\ & \left((d-b)\mathfrak{F}_{1,\ 1}(1) + t_m\mathfrak{F}_{1,\ 2}(1)\right) - t_m(d-b)\left(\prod_{i=1}^{2}\frac{d\varphi_1^{(i)}(x)}{dx}\right)\mathfrak{F}_{1,\ 1}(2)\Bigg\}_{x=1}\end{aligned} \tag{B-9}$$

$$\begin{aligned}\alpha_3^{(2)} = {} & \hat{M}\Bigg\{t_m(d-b)\left(\frac{d\varphi_1^{(1)}(x)}{dx}\right)^3\left(1 - 2\mathfrak{F}_{1,\ 2}^2(1)\right) - \varphi_1^{(1)}(x)\left(\frac{d\varphi_1^{(1)}(x)}{dx}\right)^2 \\ & \times\left(t_m\mathfrak{F}_{1,\ 1}(1) + (d-b)\mathfrak{F}_{1,\ 2}(1)\right) + \frac{1}{2}\left(\frac{d\varphi_1^{(1)}(x)}{dx}\right)^3\left((d-b)^2 - t_m^2\right)\mathfrak{F}_{1,\ 1}(2)\Bigg\}_{x=1}\end{aligned} \tag{B-10}$$

$$\begin{aligned}\alpha_4^{(2)} = {} & \hat{M}\Bigg\{t_m(d-b)\left(\frac{d\varphi_1^{(1)}(x)}{dx}\right)\left(\frac{d\varphi_1^{(2)}(x)}{dx}\right)^2\left(1 - 2\mathfrak{F}_{1,\ 2}^2(1)\right) - \varphi_1^{(1)}(x) \\ & \times\left(\frac{d\varphi_1^{(2)}(x)}{dx}\right)^2\left(t_m\mathfrak{F}_{1,\ 1}(1) + (d-b)\mathfrak{F}_{1,\ 2}(1)\right) + \frac{1}{2}\left(\frac{d\varphi_1^{(1)}(x)}{dx}\right)\left(\frac{d\varphi_1^{(2)}(x)}{dx}\right)^2 \times\left((d-b)^2 - t_m^2\right)\mathfrak{F}_{1,\ 1}(2)\Bigg\}_{x=1}\end{aligned} \tag{B-11}$$

$$\alpha_5^{(2)} = \hat{M}\Bigg\{2t_m(d-b)\left(\frac{d\varphi_1^{(1)}(x)}{dx}\right)^2\left(\frac{d\varphi_1^{(2)}(x)}{dx}\right)\left(1-2\mathfrak{F}_{1,\,2}^2(1)\right) - 2\varphi_1^{(1)}(1) \times \prod_{i=1}^{2}\frac{d\varphi_1^{(i)}(x)}{dx}\left(t_m\mathfrak{F}_{1,\,1}(1) + (d-b)\mathfrak{F}_{1,\,2}(1)\right) + \left(\frac{d\varphi_1^{(1)}(x)}{dx}\right)^2\left(\frac{d\varphi_1^{(2)}(x)}{dx}\right)\left(\frac{d\varphi_1^{(1)}(x)}{dx}\right)^2 \times \left((d-b)^2 - t_m^2\right)\mathfrak{F}_{1,\,1}(2)\Bigg\}_{x=1} \tag{B-12}$$

$$\alpha_6^{(2)} = \hat{C}L\sum_{j=1}^{2}\int_0^1\left(\varphi_j^{(1)}(x)\right)^2 dx \tag{B-13}$$

$$\alpha_7^{(2)} = \hat{C}L\sum_{j=1}^{2}\int_0^1\prod_{i=1}^{2}\varphi_j^{(i)}(x)dx \tag{B-14}$$

$$\alpha_8^{(2)} = \frac{EA}{2}\sum_{j=1}^{2}\left(\int_0^1\left(\frac{d\varphi_j^{(1)}(x)}{dx}\right)^2 dx\right)^2 \tag{B-15}$$

$$\alpha_9^{(2)} = \frac{EA}{2}\sum_{j=1}^{2}\left(\int_0^1\left(\frac{d\varphi_j^{(2)}(x)}{dx}\right)^2 dx\right)\left(\int_0^1\prod_{i=1}^{2}\frac{d\varphi_j^{(i)}(x)}{dx}dx\right) \tag{B-16}$$

$$\alpha_{10}^{(2)} = \frac{3EA}{2}\sum_{j=1}^{2}\left(\int_0^1\left(\frac{d\varphi_j^{(1)}(x)}{dx}\right)^2 dx\right)\left(\int_0^1\prod_{i=1}^{2}\frac{d\varphi_j^{(i)}(x)}{dx}dx\right) \tag{B-17}$$

$$\alpha_{11}^{(2)} = EA\sum_{j=1}^{2}\left\{\frac{1}{2}\prod_{i=1}^{2}\int_0^1\left(\frac{d\varphi_j^{(i)}(x)}{dx}\right)^2 dx + \left(\int_0^1\prod_{i=1}^{2}\frac{d\varphi_j^{(i)}(x)}{dx}dx\right)^2\right\} \tag{B-18}$$

$$\alpha_{12}^{(2)} = \frac{EA}{2}\sum_{j=1}^{2}\left(\left.\frac{d\varphi_j^{(1)}}{dx}\right|_{x=1}\right)\left(\int_0^1\left(\frac{d\varphi_j^{(1)}(x)}{dx}\right)^2 dx\right)\left(t_m\mathfrak{F}_{j,\,1}(1) + (-1)^{j-1}(d-b)\mathfrak{F}_{j,\,1}(1)\right) \tag{B-19}$$

$$\alpha_{13}^{(2)} = \frac{EA}{2}\sum_{j=1}^{2}\left(\left.\frac{d\varphi_j^{(1)}}{dx}\right|_{x=1}\right)\left(\int_0^1\left(\frac{d\varphi_j^{(2)}(x)}{dx}\right)^2 dx\right)\left(t_m\mathfrak{F}_{j,\,1}(1) + (-1)^{j-1}(d-b)\mathfrak{F}_{j,\,2}(1)\right) \tag{B-20}$$

$$\alpha_{14}^{(2)} = EA\sum_{j=1}^{2}\left(\left.\frac{d\varphi_j^{(1)}}{dx}\right|_{x=1}\right)\left(\int_0^1\prod_{i=1}^{2}\frac{d\varphi_j^{(i)}(x)}{dx}dx\right)\left(t_m\mathfrak{F}_{j,\,1}(1) + (-1)^{j-1}(d-b)\mathfrak{F}_{j,\,2}(1)\right) \tag{B-21}$$

$$\alpha_{15}^{(2)} = EA\sum_{j=1}^{2}\int_0^1\left(\frac{d\varphi_j^{(1)}(x)}{dx}\right)^2 dx \tag{B-22}$$

$$\alpha_{16}^{(2)} = EA\sum_{j=1}^{2}\int_0^1\prod_{i=1}^{2}\frac{d\varphi_j^{(i)}(x)}{dx}dx \tag{B-23}$$

$$\alpha_{17}^{(2)} = EA\sum_{j=1}^{2}\left(\int_0^1\left(\frac{d\varphi_j^{(1)}(x)}{dx}\right)^2 dx\right)\left(2t_m\mathfrak{F}_{j,\,1}^2(0.5) + (-1)^{j-1}(d-b)\mathfrak{F}_{j,\,1}(1)\right) + \frac{EI}{L^2}\sum_{j=1}^{2}\int_0^1\left(\frac{d^2\varphi_j^{(1)}(x)}{dx^2}\right)^2 dx \tag{B-24}$$

$$\alpha_{18}^{(2)} = EA\sum_{j=1}^{2}\left(\int_0^1\prod_{i=1}^{2}\frac{d\varphi_j^{(i)}(x)}{dx}dx\right)\left(2t_m\mathfrak{F}_{j,\,1}^2(0.5) + (-1)^{j-1}(d-b)\,\mathfrak{F}_{j,\,1}(1)\right) + \frac{EI}{L^2}\sum_{j=1}^{2}\int_0^1\prod_{i=1}^{2}\frac{d^2\varphi_j^{(i)}(x)}{dx^2}dx \tag{B-25}$$

$$\alpha_{19}^{(2)} = EA\sum_{j=1}^{2}\left(\left.\frac{d\varphi_j^{(1)}(x)}{dx}\right|_{x=1}\right)\left(t_m\mathfrak{F}_{j,\ 1}(1) + (-1)^{j-1}(d-b)\mathfrak{F}_{j,\ 2}(1)\right) \tag{B-26}$$

$$\alpha_{20}^{(2)} = EA\sum_{j=1}^{2}\left(\left.\frac{d\varphi_j^{(1)}}{dx}\right|_{x=1}\right)\left(2t_m\mathfrak{F}_{j,\ 1}^2(0.5)\left(t_m\mathfrak{F}_{j,\ 1}(1) + (-1)^{j-1}(d-b)\mathfrak{F}_{j,\ 2}(1)\right)\right.$$
$$\left.+\frac{1}{2}(d-b)^2\mathfrak{F}_{j,\ 1}(2) + (-1)^{j-1}t_m(d-b)\mathfrak{F}_{j,\ 1}^2(1)\right) \tag{B-27}$$

$$\alpha_{21}^{(2)} = \rho AL\sum_{j=1}^{2}\int_0^1\varphi_j^{(1)}(x)dx \tag{B-28}$$

$$\alpha_1^{(3)} = \rho AL\sum_{j=1}^{2}\int_0^1\prod_{i=1}^{2}\varphi_j^{(i)}(x)dx + \hat{M}\left\{\prod_{i=1}^{2}\varphi_1^{(i)}(x) + \kappa^2\left(\prod_{i=1}^{2}\frac{d\varphi_1^{(i)}(x)}{dx}\right)\right.$$
$$+\left(\prod_{i=1}^{2}\frac{d\varphi_1^{(i)}(x)}{dx}\right)\left((d-b)^2\mathfrak{F}_{1,\ 1}^2(1) + t_m^2\mathfrak{F}_{1,\ 2}^2(1)\right) - \frac{d}{dx}\left(\varphi_1^{(1)}(x)\varphi_1^{(2)}(x)\right)$$
$$\left.\times((d-b)\mathfrak{F}_{1,\ 1}(1) - t_m\mathfrak{F}_{1,\ 2}(1)) - t_m(d-b)\left(\prod_{i=1}^{2}\frac{d\varphi_1^{(1)}(x)}{dx}\right)\mathfrak{F}_{1,\ 1}(2)\right\}_{x=1} \tag{B-29}$$

$$\alpha_2^{(3)} = \rho AL\sum_{j=1}^{2}\int_0^L\left(\varphi_j^{(2)}(x)\right)^2dx + \hat{M}\left\{\left(\varphi_1^{(2)}(x)\right)^2 + \kappa^2\left(\frac{d\varphi_1^{(2)}(x)}{dx}\right)^2\right.$$
$$+\left(\frac{d\varphi_1^{(2)}(x)}{dx}\right)^2\left((d-b)^2\mathfrak{F}_{1,\ 1}^2(1) + t_m^2\mathfrak{F}_{1,\ 2}^2(1)\right) - 2\varphi_1^{(2)}(x)\left(\frac{d\varphi_1^{(2)}(x)}{dx}\right)$$
$$\left.\times((d-b)\mathfrak{F}_{1,\ 1}(1) - t_m\mathfrak{F}_{1,\ 2}(1)) - t_m(d-b)\left(\frac{d\varphi_1^{(2)}(x)}{dx}\right)^2\mathfrak{F}_{1,\ 1}(2)\right\}_{x=1} \tag{B-30}$$

$$\alpha_3^{(3)} = \hat{M}\left\{t_m(d-b)\left(\frac{d\varphi_1^{(1)}(x)}{dx}\right)^2\left(\frac{d\varphi_1^{(2)}(x)}{dx}\right)\left(1 - 2\mathfrak{F}_{1,\ 2}^2(1)\right) - \varphi_1^{(2)}(x)\right.$$
$$\left.\times\left(\frac{d\varphi_1^{(1)}(x)}{dx}\right)^2(t_m\mathfrak{F}_{1,\ 1}(1) + (d-b)\mathfrak{F}_{1,\ 2}(1)) + \frac{1}{2}\left(\frac{d\varphi_1^{(1)}(x)}{dx}\right)^2\left(\frac{d\varphi_1^{(2)}(x)}{dx}\right)\times\left((d-b)^2 - t_m^2\right)\mathfrak{F}_{1,\ 1}(2)\right\}_{x=1} \tag{B-31}$$

$$\alpha_4^{(3)} = \hat{M}\left\{t_m(d-b)\left(\frac{d\varphi_1^{(2)}(x)}{dx}\right)^3\left(1 - 2\mathfrak{F}_{1,\ 2}^2(1)\right) - \varphi_1^{(2)}(x)\left(\frac{d\varphi_1^{(2)}(x)}{dx}\right)^2\right.$$
$$\left.\times(t_m\mathfrak{F}_{1,\ 1}(1) + (d-b)\mathfrak{F}_{1,\ 2}(1)) + \frac{1}{2}\left(\frac{d\varphi_1^{(2)}(x)}{dx}\right)^3\left((d-b)^2 - t_m^2\right)\mathfrak{F}_{1,\ 1}(2)\right\}_{x=1} \tag{B-32}$$

$$\alpha_5^{(3)} = \hat{M}\left\{2t_m(d-b)\left(\frac{d\varphi_1^{(1)}(x)}{dx}\right)\left(\frac{d\varphi_1^{(2)}(x)}{dx}\right)^2\left(1 - 2\mathfrak{F}_{1,\ 2}^2(1)\right) - 2\varphi_1^{(2)}(L)\right.$$
$$\left.\times\left(\prod_{i=1}^{2}\frac{d\varphi_1^{(i)}(x)}{dx}\right)(t_m\mathfrak{F}_{1,\ 1}(1) + (d-b)\mathfrak{F}_{1,\ 2}(1)) + \left(\frac{d\varphi_1^{(1)}(x)}{dx}\right)\left(\frac{d\varphi_1^{(2)}(x)}{dx}\right)^2\times\left((d-b)^2 - t_m^2\right)\mathfrak{F}_{1,\ 1}(2)\right\}_{x=1} \tag{B-33}$$

$$\alpha_6^{(3)} = \hat{C}L\sum_{j=1}^{2}\int_0^1\prod_{i=1}^{2}\varphi_j^{(i)}(x)dx \tag{B-34}$$

$$\alpha_7^{(3)} = \hat{C}L\sum_{j=1}^{2}\int_0^1\left(\varphi_j^{(2)}(x)\right)^2dx \tag{B-35}$$

$$\alpha_8^{(3)} = \frac{EA}{2}\sum_{j=1}^{2}\left(\int_0^1\left(\frac{d\varphi_j^{(1)}(x)}{dx}\right)^2dx\right)\left(\int_0^1\prod_{i=1}^{2}\frac{d\varphi_j^{(i)}(x)}{dx}d\hat{x}\right) \tag{B-36}$$

$$\alpha_9^{(3)} = \frac{EA}{2}\sum_{j=1}^{2}\left(\int_0^L\left(\frac{d\varphi_j^{(2)}(x)}{dx}\right)^2dx\right)^2 \tag{B-37}$$

$$\alpha_{10}^{(3)} = \frac{EA}{2}\sum_{j=1}^{2}\left\{\prod_{i=1}^{2}\int_0^1\left(\frac{d\varphi_j^{(i)}(x)}{dx}\right)^2dx + \left(\int_0^1\prod_{i=1}^{2}\frac{d\varphi_j^{(i)}(x)}{dx}dx\right)^2\right\} \tag{B-38}$$

$$\alpha_{11}^{(3)} = \frac{3EA}{2}\sum_{j=1}^{2}\left(\int_0^1\left(\frac{d\varphi_j^{(2)}(x)}{dx}\right)^2dx\right)\left(\int_0^1\prod_{i=1}^{2}\frac{d\varphi_j^{(i)}(x)}{dx}dx\right) \tag{B-39}$$

$$\alpha_{12}^{(3)} = \frac{EA}{2}\sum_{j=1}^{2}\left(\left.\frac{d\varphi_j^{(2)}}{dx}\right|_{x=1}\right)\left(\int_0^L\left(\frac{d\varphi_j^{(2)}(x)}{dx}\right)^2dx\right)\left(t_m\mathfrak{F}_{j,\,1}(1) + (-1)^{j-1}(d-b)\mathfrak{F}_{j,\,2}(1)\right) \tag{B-40}$$

$$\alpha_{13}^{(3)} = \frac{EA}{2}\sum_{j=1}^{2}\left(\left.\frac{d\varphi_j^{(2)}}{dx}\right|_{x=1}\right)\left(\int_0^L\left(\frac{d\varphi_j^{(2)}(x)}{dx}\right)^2dx\right)\left(t_m\mathfrak{F}_{j,\,1}(1) + (-1)^{j-1}(d-b)\mathfrak{F}_{j,\,2}(1)\right) \tag{B-41}$$

$$\alpha_{14}^{(3)} = EA\sum_{j=1}^{2}\left(\left.\frac{d\varphi_j^{(2)}}{dx}\right|_{x=1}\right)\left(\int_0^1\prod_{i=1}^{2}\frac{d\varphi_j^{(i)}(x)}{dx}dx\right)\left(t_m\mathfrak{F}_{j,\,1}(1) + (-1)^{j-1}(d-b)\mathfrak{F}_{j,\,2}(1)\right) \tag{B-42}$$

$$\alpha_{15}^{(3)} = EA\sum_{j=1}^{2}\int_0^1\prod_{i=1}^{2}\frac{d\varphi_j^{(i)}(x)}{dx}dx \tag{B-43}$$

$$\alpha_{16}^{(3)} = EA\sum_{j=1}^{2}\int_0^1\left(\frac{d\varphi_j^{(2)}(x)}{dx}\right)^2dx \tag{B-44}$$

$$\alpha_{17}^{(3)} = EA\sum_{j=1}^{2}\left(\int_0^1\prod_{i=1}^{2}\frac{d\varphi_j^{(i)}(x)}{dx}dx\right)\left(2t_m\mathfrak{F}_{j,\,1}^2(0.5) + (-1)^{j-1}(d-b)\mathfrak{F}_{j,\,1}(1)\right)$$
$$+\frac{EI}{L^2}\sum_{j=1}^{2}\int_0^1\prod_{i=1}^{2}\frac{d^2\varphi_j^{(i)}(x)}{dx^2}dx \tag{B-45}$$

$$\alpha_{18}^{(3)} = EA\sum_{j=1}^{2}\left(\int_0^1\left(\frac{d\varphi_j^{(2)}(x)}{dx}\right)^2dx\right)\left(2t_m\mathfrak{F}_{j,\,1}^2(0.5) + (-1)^{j-1}(d-b)\mathfrak{F}_{j,\,1}(1)\right)$$
$$+\frac{EI}{L^2}\sum_{j=1}^{2}\int_0^1\left(\frac{d^2\varphi_j^{(2)}(x)}{dx^2}\right)^2dx \tag{B-46}$$

$$\alpha_{19}^{(3)} = EA\sum_{j=1}^{2}\left(\left.\frac{d\varphi_j^{(2)}}{dx}\right|_{x=1}\right)\left(t_m\mathfrak{F}_{j,\,1}(1) + (-1)^{j-1}(d-b)\mathfrak{F}_{j,\,2}(1)\right) \tag{B-47}$$

$$\alpha_{20}^{(3)} = EA\sum_{j=1}^{2}\left(\left.\frac{d\varphi_j^{(2)}}{dx}\right|_{x=1}\right)\Big(2t_m\mathfrak{F}_{j,\ 1}^2(0.5)\big(t_m\mathfrak{F}_{j,\ 1}(1)+(-1)^{j-1}(d-b)\mathfrak{F}_{j,\ 2}(1)\big)$$

$$+\frac{1}{2}(d-b)^2\mathfrak{F}_{j,\ 1}(2)+(-1)^{j-1}t_m(d-b)\mathfrak{F}_{j,\ 1}^2(1)\Big) \tag{B-48}$$

$$\alpha_{21}^{(3)} = \rho AL\sum_{j=1}^{2}\int_0^1 \varphi_j^{(2)}(x)dx \tag{B-49}$$

Finally, using (II-1)-(II-49), the parameters $\lambda_{ij,k}^{(l)}(q_1,q_2)$ and $\lambda_{\dot{s}}^{(l)}$ are defined as given in (II-50). Note that those coefficients not compiled in these equations are entirely zero.

$$\lambda_{00,1}^{(1)}=\frac{\alpha_6^{(1)}}{\alpha_5^{(1)}},\ \lambda_{20,1}^{(1)}=\frac{\alpha_2^{(1)}}{\alpha_5^{(1)}},\ \lambda_{11,1}^{(1)}=\frac{\alpha_4^{(1)}}{\alpha_5^{(1)}},\ \lambda_{02,1}^{(1)}=\frac{\alpha_3^{(1)}}{\alpha_5^{(1)}}$$

$$\lambda_{10,1}^{(2)}=1,\ \lambda_{01,1}^{(2)}=\frac{\alpha_2^{(2)}}{\alpha_1^{(2)}},\ \lambda_{10,2}^{(2)}=\frac{\alpha_6^{(2)}}{\alpha_1^{(2)}}\sqrt{\frac{L\alpha_1^{(1)}}{\alpha_5^{(1)}}},\ \lambda_{20,2}^{(2)}=\frac{\alpha_3^{(2)}}{\alpha_1^{(2)}}$$

$$\lambda_{01,2}^{(2)}=\frac{\alpha_7^{(2)}}{\alpha_1^{(2)}}\sqrt{\frac{L\alpha_1^{(1)}}{\alpha_5^{(1)}}},\ \lambda_{11,2}^{(2)}=\frac{\alpha_5^{(2)}}{\alpha_1^{(2)}},\ \lambda_{02,2}^{(2)}=\frac{\alpha_4^{(2)}}{\alpha_1^{(2)}},\ \lambda_{00,3}^{(2)}=\frac{\alpha_1^{(1)}\alpha_{20}^{(2)}}{\alpha_1^{(2)}\alpha_5^{(1)}}$$

$$\lambda_{10,3}^{(2)}=\frac{\alpha_1^{(1)}\alpha_{17}^{(2)}}{\alpha_1^{(2)}\alpha_5^{(1)}},\ \lambda_{20,3}^{(2)}=\frac{\alpha_1^{(1)}\alpha_{12}^{(2)}}{\alpha_1^{(2)}\alpha_5^{(1)}},\ \lambda_{30,3}^{(2)}=\frac{\alpha_1^{(1)}\alpha_8^{(2)}}{\alpha_1^{(2)}\alpha_5^{(1)}},\ \lambda_{01,3}^{(2)}=\frac{\alpha_1^{(1)}\alpha_{18}^{(2)}}{\alpha_1^{(2)}\alpha_5^{(1)}}$$

$$\lambda_{11,3}^{(2)}=\frac{\alpha_1^{(1)}\alpha_{14}^{(2)}}{\alpha_1^{(2)}\alpha_5^{(1)}},\ \lambda_{21,3}^{(2)}=\frac{\alpha_1^{(1)}\alpha_{10}^{(2)}}{\alpha_1^{(2)}\alpha_5^{(1)}},\ \lambda_{02,3}^{(2)}=\frac{\alpha_1^{(1)}\alpha_{13}^{(2)}}{\alpha_1^{(2)}\alpha_5^{(1)}},\ \lambda_{12,3}^{(2)}=\frac{\alpha_1^{(1)}\alpha_{11}^{(2)}}{\alpha_1^{(2)}\alpha_5^{(1)}}$$

$$\lambda_{03,3}^{(2)}=\frac{\alpha_1^{(1)}\alpha_9^{(2)}}{\alpha_1^{(2)}\alpha_5^{(1)}},\ \lambda_{00,4}^{(2)}=\frac{\alpha_1^{(1)}\alpha_{19}^{(2)}}{\alpha_1^{(2)}\alpha_5^{(1)}},\ \lambda_{10,4}^{(2)}=\frac{\alpha_1^{(1)}\alpha_{15}^{(2)}}{\alpha_1^{(2)}\alpha_5^{(1)}},\ \lambda_{01,4}^{(2)}=\frac{\alpha_1^{(1)}\alpha_{16}^{(2)}}{\alpha_1^{(2)}\alpha_5^{(1)}}$$

$$\lambda_{\dot{s}}^{(2)}=\frac{\alpha_{21}^{(2)}}{\alpha_1^{(2)}},\ \lambda_{10,1}^{(3)}=\frac{\alpha_1^{(3)}}{\alpha_2^{(3)}},\ \lambda_{01,1}^{(3)}=1,\ \lambda_{10,2}^{(3)}=\frac{\alpha_6^{(3)}}{\alpha_2^{(3)}}\sqrt{\frac{L\alpha_1^{(1)}}{\alpha_5^{(1)}}}$$

$$\lambda_{20,2}^{(3)}=\frac{\alpha_3^{(3)}}{\alpha_2^{(3)}},\ \lambda_{01,2}^{(3)}=\frac{\alpha_7^{(3)}}{\alpha_2^{(3)}}\sqrt{\frac{L\alpha_1^{(1)}}{\alpha_5^{(1)}}},\ \lambda_{11,2}^{(3)}=\frac{\alpha_5^{(3)}}{\alpha_2^{(3)}},\ \lambda_{02,2}^{(3)}=\frac{\alpha_4^{(3)}}{\alpha_2^{(3)}}$$

$$\lambda_{00,3}^{(3)}=\frac{\alpha_1^{(1)}\alpha_{20}^{(3)}}{\alpha_2^{(3)}\alpha_5^{(1)}},\ \lambda_{10,3}^{(3)}=\frac{\alpha_1^{(1)}\alpha_{17}^{(3)}}{\alpha_2^{(3)}\alpha_5^{(1)}},\ \lambda_{20,3}^{(3)}=\frac{\alpha_1^{(1)}\alpha_{12}^{(3)}}{\alpha_2^{(3)}\alpha_5^{(1)}},\ \lambda_{30,3}^{(3)}=\frac{\alpha_1^{(1)}\alpha_8^{(3)}}{\alpha_2^{(3)}\alpha_5^{(1)}}$$

$$\lambda_{01,3}^{(3)}=\frac{\alpha_1^{(1)}\alpha_{18}^{(3)}}{\alpha_2^{(3)}\alpha_5^{(1)}},\ \lambda_{11,3}^{(3)}=\frac{\alpha_1^{(1)}\alpha_{14}^{(3)}}{\alpha_2^{(3)}\alpha_5^{(1)}},\ \lambda_{21,3}^{(3)}=\frac{\alpha_1^{(1)}\alpha_{10}^{(3)}}{\alpha_2^{(3)}\alpha_5^{(1)}},\ \lambda_{02,3}^{(3)}=\frac{\alpha_1^{(1)}\alpha_{13}^{(3)}}{\alpha_2^{(3)}\alpha_5^{(1)}}$$

$$\lambda_{12,3}^{(3)}=\frac{\alpha_1^{(1)}\alpha_{11}^{(3)}}{\alpha_2^{(3)}\alpha_5^{(1)}},\ \lambda_{03,3}^{(3)}=\frac{\alpha_1^{(1)}\alpha_9^{(3)}}{\alpha_2^{(3)}\alpha_5^{(1)}},\ \lambda_{00,4}^{(3)}=\frac{\alpha_1^{(1)}\alpha_{19}^{(3)}}{\alpha_2^{(3)}\alpha_5^{(1)}},\ \lambda_{10,4}^{(3)}=\frac{\alpha_1^{(1)}\alpha_{15}^{(3)}}{\alpha_2^{(3)}\alpha_5^{(1)}}$$

$$\lambda_{01,4}^{(3)}=\frac{\alpha_1^{(1)}\alpha_{16}^{(3)}}{\alpha_2^{(3)}\alpha_5^{(1)}},\ \lambda_{\dot{s}}^{(3)}=\frac{\alpha_{21}^{(3)}}{\alpha_2^{(3)}} \tag{B-50}$$

Appendix C. Definition of the coefficients $\gamma_{i,j}^{(k)}$, γ_c and γ_3

To present the coefficients $\gamma_{i,j}^{(k)}$, γ_c and γ_3 more conveniently, we first define $\beta_i^{(j)}$s as follows.

$$\beta_1^{(1)} = \hat{M} \tag{C-1}$$

$$\beta_2^{(1)} = -\frac{t_m}{24} EA \sum_{j=1}^{2} \left(\left. \frac{d\varphi_j^{(1)}}{dx} \right|_{x=1} \right)^4 \tag{C-2}$$

$$\beta_3^{(1)} = \frac{(d-b)}{6} EA \sum_{j=1}^{2} (-1)^j \left(\left. \frac{d\varphi_j^{(1)}}{dx} \right|_{x=1} \right)^3 \tag{C-3}$$

$$\beta_4^{(1)} = \frac{EA}{2} \sum_{j=1}^{2} \left\{ t_m \left(\left. \frac{d\varphi_j^{(1)}}{dx} \right|_{x=1} \right)^2 + \int_0^1 \left(\frac{d\varphi_j^{(1)}(x)}{dx} \right)^2 dx \right\} \tag{C-4}$$

$$\beta_5^{(1)} = (d-b) EA \sum_{j=1}^{2} (-1)^{j-1} \left(\left. \frac{d\varphi_j^{(1)}}{dx} \right|_{x=1} \right) \tag{C-5}$$

$$\beta_6^{(1)} = 2EA \tag{C-6}$$

$$\beta_1^{(2)} = \rho AL \sum_{j=1}^{2} \int_0^L \left(\varphi_j^{(1)}(x)\right)^2 dx + \hat{M} \left[2t_m \varphi_1^{(1)}(x) \left(\frac{d\varphi_1^{(1)}(x)}{dx} \right) + t_m^2 \left(\frac{d\varphi_1^{(1)}(x)}{dx} \right)^2 + \left(\varphi_1^{(1)}(x)\right)^2 + \kappa^2 \left(\frac{d\varphi_1^{(1)}(x)}{dx} \right)^2 \right]_{x=1} \tag{C-7}$$

$$\beta_2^{(2)} = -2\hat{M}(d-b) \left[\left(\frac{d\varphi_1^{(1)}(x)}{dx} \right)^2 \varphi_1^{(1)}(x) + t_m \left(\frac{d\varphi_1^{(1)}(x)}{dx} \right)^3 \right]_{x=1} \tag{C-8}$$

$$\beta_3^{(2)} = -\hat{M} \left(\left. \frac{d\varphi_1^{(1)}}{dx} \right|_{x=1} \right)^3 \left[t_m \varphi_1^{(1)}(x) + \left(\frac{d\varphi_1^{(1)}(x)}{dx} \right) \left(t_m^2 - (d-b)^2 \right) \right]_{x=1} \tag{C-9}$$

$$\beta_4^{(2)} = \frac{\hat{M}(d-b)}{3} \left(\left. \frac{d\varphi_1^{(1)}}{dx} \right|_{x=1} \right)^4 \left[\varphi_1^{(1)}(x) + 4t_m \left(\frac{d\varphi_1^{(1)}(x)}{dx} \right) \right]_{x=1} \tag{C-10}$$

$$\beta_5^{(2)} = \frac{\hat{M}}{12} \left(\left. \frac{d\varphi_1^{(1)}}{dx} \right|_{x=1} \right)^5 \left[t_m \varphi_1^{(1)}(x) + 4 \left(\frac{d\varphi_1^{(1)}(x)}{dx} \right) \left(t_m^2 - (d-b)^2 \right) \right]_{x=1} \tag{C-11}$$

$$\beta_6^{(2)} = \hat{C} L \sum_{j=1}^{2} \int_0^1 \left(\varphi_j^{(1)}(x)\right)^2 dx \tag{C-12}$$

$$\beta_7^{(2)} = -\hat{M}(d-b) \left(\left. \frac{d\varphi_1^{(1)}}{dx} \right|_{x=1} \right)^2 \left[\varphi_1^{(1)}(x) + t_m \left(\frac{d\varphi_1^{(1)}(x)}{dx} \right) \right]_{x=1} \tag{C-13}$$

$$\beta_8^{(2)} = -\hat{M} \left(\left. \frac{d\varphi_1^{(1)}}{dx} \right|_{x=1} \right)^3 \left[t_m \varphi_1^{(1)}(x) + \left(\frac{d\varphi_1^{(1)}(x)}{dx} \right) \left(t_m^2 - (d-b)^2 \right) \right]_{x=1} \tag{C-14}$$

$$\beta_9^{(2)} = \frac{\hat{M}(d-b)}{2} \left(\left. \frac{d\varphi_1^{(1)}}{dx} \right|_{x=1} \right)^4 \left[\varphi_1^{(1)}(x) + 4t_m \left(\frac{d\varphi_1^{(1)}(x)}{dx} \right) \right]_{x=1} \tag{C-15}$$

$$\beta_{10}^{(2)} = \frac{\hat{M}}{6} \left(\left. \frac{d\varphi_1^{(1)}}{dx} \right|_{x=1} \right)^5 \left[t_m \varphi_1^{(1)}(x) + 4 \left(\frac{d\varphi_1^{(1)}(x)}{dx} \right) \left(t_m^2 - (d-b)^2 \right) \right]_{x=1} \tag{C-16}$$

$$\beta_{11}^{(2)} = -\frac{\hat{M}\left(\hat{d} - \hat{b}\right)}{24} \left(\left. \frac{d\varphi_1^{(1)}}{dx} \right|_{x=1} \right)^6 \left[\varphi_1^{(1)}(x) + 16t_m \left(\frac{d\varphi_1^{(1)}(x)}{dx} \right) \right]_{x=1} \tag{C-17}$$

$$\beta_{12}^{(2)} = \frac{EI}{L^2}\sum_{j=1}^{2}\int_0^1 \left(\frac{d^2\varphi_j^{(1)}(x)}{dx^2}\right)^2 dx + (d-b)^2 EA\sum_{j=1}^{2}\left(\left.\frac{d\varphi_1^{(1)}}{dx}\right|_{x=1}\right)^2 \tag{C-18}$$

$$\beta_{13}^{(2)} = \frac{3(d-b)}{2}EA\sum_{j=1}^{2}(-1)^{j-1}\left\{\left(\left.\frac{d\varphi_j^{(1)}}{dx}\right|_{x=1}\right)\int_0^1\left(\frac{d\varphi_j^{(1)}(x)}{dx}\right)^2 dx + t_m\left(\left.\frac{d\varphi_j^{(1)}}{dx}\right|_{x=1}\right)^3\right\} \tag{C-19}$$

$$\beta_{14}^{(2)} = \frac{EA}{2}\sum_{j=1}^{2}\left\{\left(\int_0^1\left(\frac{d\varphi_j^{(1)}(x)}{dx}\right)^2 dx\right)^2 + t_m\left(\left.\frac{d\varphi_j^{(1)}}{dx}\right|_{x=1}\right)^2\int_0^1\left(\frac{d\varphi_j^{(1)}(x)}{dx}\right)^2 dx + \left(\left.\frac{d\varphi_j^{(1)}}{dx}\right|_{x=1}\right)^4\left(t_m^2 - \frac{4(d-b)^2}{3}\right)\right\} \tag{C-20}$$

$$\beta_{15}^{(2)} = \frac{5(d-b)}{8}EA\sum_{j=1}^{2}(-1)^{j}\left\{\frac{2}{3}\left(\left.\frac{d\varphi_j^{(1)}}{dx}\right|_{x=1}\right)^3\int_0^1\left(\frac{d\varphi_j^{(1)}(x)}{dx}\right)^2 dx + t_m\left(\left.\frac{d\varphi_j^{(1)}}{dx}\right|_{x=1}\right)^5\right\} \tag{C-21}$$

$$\beta_{16}^{(2)} = -\frac{t_m}{8}EA\sum_{j=1}^{2}\left(\left.\frac{d\varphi_j^{(1)}}{dx}\right|_{x=1}\right)^4\int_0^1\left(\frac{d\varphi_j^{(1)}(x)}{dx}\right)^2 dx \tag{C-22}$$

$$\beta_{17}^{(2)} = \frac{(d-b)}{48}EA\sum_{j=1}^{2}(-1)^{j-1}\left(\left.\frac{d\varphi_j^{(1)}}{dx}\right|_{x=1}\right)^5\int_0^1\left(\frac{d\varphi_j^{(1)}(x)}{dx}\right)^2 dx \tag{C-23}$$

$$\beta_{18}^{(2)} = (d-b)EA\sum_{j=1}^{2}(-1)^{j-1}\left(\left.\frac{d\varphi_j^{(1)}}{dx}\right|_{x=1}\right) \tag{C-24}$$

$$\beta_{19}^{(2)} = EA\sum_{j=1}^{2}\left\{t_m\left(\left.\frac{d\varphi_j^{(1)}}{dx}\right|_{x=1}\right)^2 + \int_0^1\left(\frac{d\varphi_j^{(1)}(x)}{dx}\right)^2 dx\right\} \tag{C-25}$$

$$\beta_{20}^{(2)} = \frac{(d-b)}{2}EA\sum_{j=1}^{2}(-1)^{j}\left(\left.\frac{d\varphi_j^{(1)}}{dx}\right|_{x=1}\right)^3 \tag{C-26}$$

$$\beta_{21}^{(2)} = -\frac{t_m}{6}EA\sum_{j=1}^{2}\left(\left.\frac{d\varphi_j^{(1)}}{dx}\right|_{x=1}\right)^4 \tag{C-27}$$

$$\beta_{22}^{(2)} = \frac{(d-b)}{24}EA\sum_{j=1}^{2}(-1)^{j-1}\left(\left.\frac{d\varphi_j^{(1)}}{dx}\right|_{x=1}\right)^5 \tag{C-28}$$

$$\beta_{23}^{(2)} = \rho AL\sum_{j=1}^{2}\int_0^1\varphi_j^{(1)}(x)dx \tag{C-29}$$

Now, the parameters $\gamma_{i,j}^{(k)}$ are defined in terms of $\beta_i^{(j)}$s as given in (III-30).

$$\gamma_{1,1}^{(1)} = \frac{\beta_5^{(1)}}{\beta_6^{(1)}},\ \gamma_{2,1}^{(1)} = \frac{\beta_4^{(1)}}{\beta_6^{(1)}},\ \gamma_{3,1}^{(1)} = \frac{\beta_3^{(1)}}{\beta_6^{(1)}},\ \gamma_{4,1}^{(1)} = \frac{\beta_2^{(1)}}{\beta_6^{(1)}}$$

$$\gamma_{1,1}^{(2)} = \frac{\beta_2^{(2)}}{\beta_1^{(2)}},\ \gamma_{2,1}^{(2)} = \frac{\beta_3^{(2)}}{\beta_1^{(2)}},\ \gamma_{3,1}^{(2)} = \frac{\beta_4^{(2)}}{\beta_1^{(2)}},\ \gamma_{4,1}^{(2)} = \frac{\beta_5^{(2)}}{\beta_1^{(2)}}$$

$$\gamma_c = \frac{\beta_6^{(2)}}{\beta_1^{(2)}}\sqrt{L\frac{\beta_1^{(1)}}{\beta_6^{(1)}}},\ \gamma_{0,2}^{(2)} = \frac{\beta_7^{(2)}}{\beta_1^{(2)}},\ \gamma_{1,2}^{(2)} = \frac{\beta_8^{(2)}}{\beta_1^{(2)}},\ \gamma_{2,2}^{(2)} = \frac{\beta_9^{(2)}}{\beta_1^{(2)}}$$

$$\gamma_{3,2}^{(2)} = \frac{\beta_{10}^{(2)}}{\beta_1^{(2)}},\ \gamma_{4,2}^{(2)} = \frac{\beta_{11}^{(2)}}{\beta_1^{(2)}},\ \gamma_{1,3}^{(2)} = \frac{\beta_{12}^{(2)}\beta_1^{(1)}}{\beta_1^{(2)}\beta_6^{(1)}},\ \gamma_{2,3}^{(2)} = \frac{\beta_{13}^{(2)}\beta_1^{(1)}}{\beta_1^{(2)}\beta_6^{(1)}}$$

$$\gamma_{3,3}^{(2)} = \frac{\beta_{14}^{(2)}\beta_1^{(1)}}{\beta_1^{(2)}\beta_6^{(1)}},\ \gamma_{4,3}^{(2)} = \frac{\beta_{15}^{(2)}\beta_1^{(1)}}{\beta_1^{(2)}\beta_6^{(1)}},\ \gamma_{5,3}^{(2)} = \frac{\beta_{16}^{(2)}\beta_1^{(1)}}{\beta_1^{(2)}\beta_6^{(1)}},\ \gamma_{6,3}^{(2)} = \frac{\beta_{17}^{(2)}\beta_1^{(1)}}{\beta_1^{(2)}\beta_6^{(1)}}$$

$$\gamma_{0,4}^{(2)} = \frac{\beta_{18}^{(2)}\beta_1^{(1)}}{\beta_1^{(2)}\beta_6^{(1)}},\ \gamma_{1,4}^{(2)} = \frac{\beta_{19}^{(2)}\beta_1^{(1)}}{\beta_1^{(2)}\beta_6^{(1)}},\ \gamma_{2,4}^{(2)} = \frac{\beta_{20}^{(2)}\beta_1^{(1)}}{\beta_1^{(2)}\beta_6^{(1)}},\ \gamma_{3,4}^{(2)} = \frac{\beta_{21}^{(2)}\beta_1^{(1)}}{\beta_1^{(2)}\beta_6^{(1)}}$$

$$\gamma_{4,4}^{(2)} = \frac{\beta_{22}^{(2)}\beta_1^{(1)}}{\beta_1^{(2)}\beta_6^{(1)}},\ \gamma_3 = \Omega^2 \frac{\widehat{\mathbb{Z}}_b}{L}\frac{\beta_{23}^{(2)}}{\beta_1^{(2)}} \tag{C-30}$$

References

[1] S. Awtar, T.T. Trutna, J.M. Nielsen, R. Abani, J. Geiger, FlexDex™: a minimally invasive surgical tool with enhanced dexterity and intuitive control, J Med Device 4 (2010) 035003.
[2] M.I. Frecker, K.M. Powell, R. Haluck, Design of a multifunctional compliant instrument for minimally invasive surgery, J Biomech Eng 127 (2005) 990–993.
[3] V. Gupta, R. Perathara, A.K. Chaurasiya, J.P. Khatait, Design and analysis of a flexure based passive gripper, Precision Engineering 56 (2019) 537–548.
[4] K. Cai, Y. Tian, X. Liu, D. Zhang, J. Shang, B. Shirinzadeh, Development and control methodologies for 2-DOF micro/nano positioning stage with high out-of-plane payload capacity, Robot Comput Integr Manuf 56 (2019) 95–105.
[5] H. Li, G. Hao, Position-space-based design of a symmetric spatial translational compliant mechanism for micro-/nano-manipulation, Micromachines (Basel) 9 (2018) 189.
[6] R. Wang, X. Zhou, G. Meng, Probabilistic robustness analysis on the planar parasitic motions of flexural mechanisms with uncertain manufacturing imperfectness, Sensors and Actuators A: Physical 294 (2019) 154–163.
[7] S. Meninger, J.O. Mur-Miranda, R. Amirtharajah, A. Chandrakasan, J.H. Lang, Vibration-to-electric energy conversion, IEEE Transactions on Very Large Scale Integration (VLSI) Systems 9 (2001) 64–76.
[8] S. Wen, Q. Xu, Design of a Novel Piezoelectric Energy Harvester Based on Integrated Multi-Stage Force Amplification Frame, IEEE/ASME Transactions on Mechatronics (2019).
[9] Y.-l. Yang, Y.-d. Wei, J.-q. Lou, L. Fu, X.-w. Zhao, Nonlinear dynamic analysis and optimal trajectory planning of a high-speed macro-micro manipulator, J Sound Vib 405 (2017) 112–132.
[10] M. Bakhtiari-Shahri, H. Moeenfard, Topology optimization of fundamental compliant mechanisms using a novel asymmetric beam flexure, International Journal of Mechanical Sciences 135 (2018) 383–397.
[11] H. Malaeke, H. Moeenfard, A novel flexure beam module with low stiffness loss in compliant mechanisms, Precision Engineering 48 (2017) 216–233.
[12] P.P. Valentini, M. Cirelli, E. Pennestrì, Second-order approximation pseudo-rigid model of flexure hinge with parabolic variable thickness, Mech Mach Theory 136 (2019) 178–189.
[13] S. Šalinić, A. Nikolić, A new pseudo-rigid-body model approach for modeling the quasi-static response of planar flexure-hinge mechanisms, Mech Mach Theory 124 (2018) 150–161.
[14] P. Liu, P. Yan, Modeling and analysis of beam flexure based double parallel guiding mechanisms: a modified pseudo-rigid-body approach, ASME 2016 International Design Engineering Technical Conferences and Computers and Information in Engineering Conference, 2016.
[15] X. Zhang, Q. Xu, Design and analysis of a 2-DOF compliant gripper with constant-force flexure mechanism, Journal of Micro-Bio Robotics 15 (2019) 31–42.
[16] A. Cammarata, M. Lacagnina, G. Sequenzia, Alternative elliptic integral solution to the beam deflection equations for the design of compliant mechanisms, International Journal on Interactive Design and Manufacturing (IJIDeM) 13 (2019) 499–505.
[17] G. Chen, F. Ma, G. Hao, W. Zhu, Modeling large deflections of initially curved beams in compliant mechanisms using chained beam constraint model, J Mech Robot 11 (2019) 011002.
[18] G. Chen, R. Bai, Modeling large spatial deflections of slender bisymmetric beams in compliant mechanisms using chained spatial-beam constraint model, J Mech Robot 8 (2016) 041011.
[19] S. Sen, "Beam Constraint Model: generalized Nonlinear Closed-form Modeling of Beam Flexures for Flexure Mechanism Design," 2013.
[20] M. Radgolchin, H. Moeenfard, A constraint model for beam flexure modules with an intermediate semi-rigid element, International Journal of Mechanical Sciences 122 (2017) 167–183.
[21] R. Bai, S. Awtar, G. Chen, A closed-form model for nonlinear spatial deflections of rectangular beams in intermediate range, International Journal of Mechanical Sciences 160 (2019) 229–240.
[22] S. Awtar, S. Sen, A generalized constraint model for two-dimensional beam flexures: nonlinear load-displacement formulation, Journal of Mechanical Design 132 (2010) 081008.
[23] S. Awtar, S. Sen, A generalized constraint model for two-dimensional beam flexures: nonlinear strain energy formulation, Journal of Mechanical Design 132 (2010) 081009.
[24] S. Awtar, K. Shimotsu, S. Sen, Elastic averaging in flexure mechanisms: a three-beam parallelogram flexure case study, J Mech Robot 2 (2010) 041006.
[25] S. Sen, S. Awtar, A closed-form nonlinear model for the constraint characteristics of symmetric spatial beams, Journal of Mechanical Design 135 (2013) 031003.
[26] F. Ma, G. Chen, Modeling large planar deflections of flexible beams in compliant mechanisms using chained beam-constraint-Model, J Mech Robot 8 (2016) 021018.
[27] H. Moeenfard, S. Awtar, Modeling geometric nonlinearities in the free vibration of a planar beam flexure with a tip mass, Journal of Mechanical Design 136 (2014) 044502.
[28] H. Malaeke, H. Moeenfard, Analytical modeling of large amplitude free vibration of non-uniform beams carrying a both transversely and axially eccentric tip mass, J Sound Vib 366 (2016) 211–229.
[29] C.J. Silva, M.F. Daqaq, Nonlinear flexural response of a slender cantilever beam of constant thickness and linearly-varying width to a primary resonance excitation, J Sound Vib 389 (2017) 438–453.
[30] M.R. Sayag, E.H. Dowell, Linear versus nonlinear response of a cantilevered beam under harmonic base excitation: theory and experiment, J Appl Mech 83 (2016) 101002.
[31] M. Radgolchin, H. Moeenfard, Analytical modeling of nonlinear flexural-extensional vibration of flexure beams with an interconnected compliant element, Mech Res Commun 89 (2018) 23–33.
[32] J. Banerjee, Dynamic stiffness formulation for structural elements: a general approach, Comput Struct 63 (1997) 101–103.
[33] J. Banerjee, Free vibration of centrifugally stiffened uniform and tapered beams using the dynamic stiffness method, J Sound Vib 233 (2000) 857–875.

[34] J. Banerjee, D. Kennedy, Dynamic stiffness method for inplane free vibration of rotating beams including Coriolis effects, J Sound Vib 333 (2014) 7299–7312.
[35] M. Ling, S. Chen, Q. Li, G. Tian, Dynamic stiffness matrix for free vibration analysis of flexure hinges based on non-uniform Timoshenko beam, J Sound Vib 437 (2018) 40–52.
[36] Q. Zhou, N. Toombs, P. Ferreira, Dynamics modeling and verification of a large-displacement precision preloaded-flexure stage, J Manuf Process (2019).
[37] M. Ling, A general two-port dynamic stiffness model and static/dynamic comparison for three bridge-type flexure displacement amplifiers, Mech Syst Signal Process 119 (2019) 486–500.
[38] A. Pagani, M. Boscolo, J. Banerjee, E. Carrera, Exact dynamic stiffness elements based on one-dimensional higher-order theories for free vibration analysis of solid and thin-walled structures, J Sound Vib 332 (2013) 6104–6127.
[39] A.A. Tanksale, P.S. Gandhi, On novel dynamic displacement amplification using compliant mechanisms, ASME 2018 International Mechanical Engineering Congress and Exposition, 2019.
[40] H. van der Deijl, D. de Klerk, J.L. Herder, D.F. Machekposhti, Dynamics of a compliant transmission mechanism between parallel rotational axes, Mech Mach Theory 139 (2019) 251–269.
[41] Z. Zhang, X. Yang, P. Yan, Large dynamic range tracking of an XY compliant nanomanipulator with cross-axis coupling reduction, Mech Syst Signal Process 117 (2019) 757–770.
[42] L. Cui, C. Okwudire, S. Awtar, Modeling complex nonminimum phase zeros in flexure mechanisms, J Dyn Syst Meas Control 139 (2017).
[43] H. Sadeghian, N. Koster, T. van den Dool, Introduction of a high throughput SPM for defect inspection and process control, Metrology, Inspection, and Process Control for Microlithography XXVII, 2013.
[44] A. Mohammadi, A.G. Fowler, Y.K. Yong, S.R. Moheimani, A feedback controlled MEMS nanopositioner for on-chip high-speed AFM, Journal of Microelectromechanical Systems 23 (2013) 610–619.
[45] S.S. Rao, Vibration of Continuous Systems, 464, Wiley Online Library, 2007.
[46] Y. Yang, L. Jézéquel, O. Dessombz, P. Bristiel, O. Sauvage, Modelization of boundary friction damping induced by second-order bending strain, J Sound Vib 446 (2019) 113–128.
[47] A.H. Nayfeh, D.T. Mook, P. Holmes, Nonlinear oscillations, American Society of Mechanical Engineers Digital Collection, 1980.
[48] J.N. Reddy, Energy Principles and Variational Methods in Applied Mechanics, John Wiley & Sons, 2017.
[49] M. Rezaei, R. Talebitooti, S. Rahmanian, Efficient energy harvesting from nonlinear vibrations of PZT beam under simultaneous resonances, Energy 182 (2019) 369–380.